WEB LINK FOR HIGH RESOLUTION DOCUMENT IN FOOTNOTE
Preprint typeset using LaTeX style emulateapj v. 11/26/04

arXiv:astro-ph/0506368v1 16 Jun 2005

JET FORMATION IN BLACK HOLE ACCRETION SYSTEMS I: THEORETICAL UNIFICATION MODEL

JONATHAN C. MCKINNEY[1]

June 16, 2005

ABSTRACT

Two types of relativistic jets are suggested to form near accreting black holes: a potentially ultrarelativistic Poynting-dominated jet and a Poynting-baryon jet. One source of jet matter is electron-positron pair production, which is driven by neutrino annihilation in GRBs and photon annihilation in AGN and x-ray binaries. GRB Poynting-dominated jets are also loaded by electron-proton pairs by the collisional cascade of Fick-diffused free neutrons. We show that, for the collapsar model, the neutrino-driven enthalpy flux (classic fireball model) is probably dominated by the Blandford-Znajek energy flux, which predicts a jet Lorentz factor of $\Gamma \sim 100-1000$. We show that radiatively inefficient AGN, such as M87, are synchrotron-cooling limited to $\Gamma \sim 2-10$. Radiatively efficient x-ray binaries, such as GRS1915+105, are Compton-drag limited to $\Gamma \lesssim 2$, but the jet may be destroyed by Compton drag. However, the Poynting-baryon jet is a collimated outflow with $\Gamma \sim 1-3$. The jet from radiatively efficient systems, such as microquasar GRS1915+105, may instead be a Poynting-baryon jet that is only relativistic when the disk is geometrically thick. In a companion paper, general relativistic hydromagnetic simulations of black hole accretion with pair creation are used to simulate jet formation in GRBs, AGN, and x-ray binaries.

Subject headings: accretion disks, black hole physics, galaxies: jets, gamma rays: bursts, X-rays : bursts, supernovae: general, neutrinos

1. INTRODUCTION

Jets are a common outcome of accretion, yet the observed jet properties, such as collimation and speed, are not uniform between systems. This is despite the fact that the basic physics (general relativistic magnetohydrodynamics (GRMHD)) to describe such systems is black hole mass-invariant. Thus, it is worth-while to determine the unifying, or minimum number of, pieces of physics that would explain most of the features of gamma-ray bursts (GRBs), x-ray binaries, and active galactic nuclei (AGN) (Ghisellini & Celotti 2002; Ghisellini 2003; Meier 2003). To understand jet *formation* requires at least explaining the origin of the energy, composition, collimation, and Lorentz factor. The goal of this paper, and the companion numerical models paper (McKinney 2005b), is to explain these for GRBs, AGN, and x-ray binaries.

Primarily we discuss two types of jets: Poynting-dominated jets typically dominated in energy flux by Poynting flux and dominated in mass by electron-positron pairs for AGN and x-ray binaries, while dominated in mass by electron-proton pairs for GRBs ; and Poynting-baryon jets with about equal Poynting flux and rest-mass flux and dominated in mass by baryons. The latter are sometimes referred to as coronal outflows due to their origin. Generically this model is similar to, e.g., Sol et al. (1989), while here the motivation is based upon the results of recent GRMHD numerical models. This two-component jet model is one key to understanding the diversity of jet observations. The Poynting-dominated jet is likely powered by the Blandford-Znajek effect, while the Poynting-baryon jet is likely powered by both Blandford-Znajek power and the release of disk gravitational binding energy (McKinney 2005a). Collimation of the polar Poynting-dominated jet may be due transfield balance against the broader Poynting-baryon jet or by self-collimating hoop stresses.

Among all the black hole accretion systems, it appears that the least unifiable is the observed emission. While the radiative physics is not black hole mass invariant, the observed differences suggest that the environment likely plays a significant role in the emission. For example, while both blazars and GRBs exhibit non-thermal emission, long-duration GRBs are harder with higher luminosity, while blazars are softer with higher luminosity (Ghirlanda et al. 2004, 2005). Also, GRBs lead to apparently most of the energy in γ-rays and less than 10% to the sub-γ-ray afterglow (Piran 2005). On the contrary, blazars apparently release only 10% in γ-rays and the rest is produced in the radio lobe (Ghisellini & Celotti 2002). Despite the difficulties in understanding the emission processes in some jet systems, the jet itself is probably produced by a universal process.

The disk *and* jet radiative physics are keys to understanding the evolution of the jet and why different systems have different terminal Lorentz factors. Through radiative annihilation of photons in AGN and x-ray binary systems, the radiative physics may illuminate the origin of jet composition by determining the electron-positron mass-loading the Poynting-lepton jet, and so the Lorentz factor of the jet. For GRBs, the radiative annihilation of neutrinos and the effect of Fick diffusion by free neutrons from the corona into the jet (Levinson & Eichler 2003) may give an understanding of the Lorentz factor of the jet and the origin of baryon-contamination.

The rest of this section briefly reviews the types of black hole accretion systems and discusses jets in each. At the end is an outline of the paper.

1.1. *GRBs*

Neutron stars and black holes are associated with the most violent of post-Big Bang events: supernovae and some gamma-ray bursts (GRBs) and probably some x-ray flashes (XRFs) (for a general review see Woosley 1993; Wheeler, Yi, Höflich, & Wang 2000). Observations of a su-

---

[1] Institute for Theory and Computation, Harvard-Smithsonian Center for Astrophysics, 60 Garden Street, MS 51, Cambridge, MA 02138, USA
High Res. Figures: `http://rainman.astro.uiuc.edu/~jon/j1.pdf`
Electronic address: jmckinney@cfa.harvard.edu

pernova light curve (SN2003dh) in the afterglow of GRB 030329 suggest that at least some long-duration GRBs are probably associated with core-collapse events (Stanek et al. 2003; Kawabata et al. 2003; Uemura et al. 2003; Hjorth et al. 2003).

Neutrino processes and magnetic fields are both important to understand core-collapse. In unraveling the mechanism by which core-collapse supernovae explode, the implementation of accurate neutrino transport has been realized to be critical to whether a supernova is produced in simulations (Messer et al. and collaborators 1998). This has thus far been interpreted to imply that highly accurate neutrino transport physics is required, but this could also mean additional physics, such as a magnetic field, could play a significant role. Indeed, all core-collapse events may be powered by MHD processes rather than neutrino processes (Leblanc & Wilson 1970; Symbalisty 1984; Woosley & Weaver 1986; Duncan & Thompson 1992; Khokhlov et al. 1999; Akiyama, Wheeler, Meier, & Lichtenstadt 2003). Core-collapse involves shearing subject to the Balbus-Hawley instability as in accretion disks (Akiyama, Wheeler, Meier, & Lichtenstadt 2003). All core-collapse explosions are significantly polarised, asymmetric, and often bi-polar indicating a strong role of rotation and a magnetic field (see, e.g., Wang & Wheeler 1996; Wheeler, Yi, Höflich, & Wang 2000; Wang, Howell, Höflich, & Wheeler 2001; Wang et al. 2002; Wang, Baade, Höflich, & Wheeler 2003, and references therein). Possible evidence for a magnetic dominated outflow has been found in GRB 021206 (Coburn & Boggs 2003), marginally consistent with a magnetic outflow directly from the inner engine (Lyutikov, Pariev, & Blandford 2003), although these observations remain controversial.

Black hole accretion is the key source of energy for many GRB models. Collapsar type models suggest that a black hole forms during the core-collapse of some relatively rapidly rotating massive stars. The typical radius of the accretion disk likely determines the duration of long-duration GRBs (Woosley 1993; Paczynski 1998; MacFadyen & Woosley 1999). An accretion disk is also formed as a result of a neutron star or black hole collisions with another stellar object (Narayan et al. 1992, 2001).

GRBs are believed to be the result of an ultrarelativistic jet. Indirect observational evidence of relativistic motion is suggested by afterglow achromatic light breaks and the "compactness problem" suggests GRB material must be ultrarelativistic with Lorentz factor $\Gamma \gtrsim 100$ to emit the observed nonthermal γ-rays (see, e.g., Piran 2005). Direct observational evidence for relativistic motion comes from radio scintillation of the ISM (Goodman 1997) and measurements of the afterglow emitting region from GRB030329 (Taylor et al. 2004a,b).

Typical GRB jet models invoke either a hot neutrino-driven jet or a cold Poynting flux-dominated jet, while both allow for comparable amounts of the accretion energy to power the jet (Popham et al. 1999). A neutrino-driven jet derives its energy from neutrino annihilation from gravitational energy and the jet is thermally accelerated. However, strong outflows can be magnetically driven (Bisnovatyi-Kogan & Ruzmaikin 1976; Lovelace 1976; Blandford 1976). In particular, black hole rotational energy can be extracted as a Poynting outflow (Blandford & Znajek 1977).

1.2. *X-ray Binaries*

Long after their formation, neutron stars and black holes often continue to produce outflows and jets (Mirabel & Rodríguez 1999). These include x-ray binaries (for a review see Lewin et al. 1995; McClintock & Remillard 2003), neutron star as pulsars (for a review see Lorimer 2001 on ms pulsars and Thorsett & Chakrabarty 1999 on radio pulsars) and soft-gamma ray repeaters (SGRs) (Thompson & Duncan 1995, 1996; Kouveliotou et al. 1999). In the case of x-ray binaries, the companion star's solar-wind or Roche-lobe forms an accretion disk. Many x-ray binaries in their hard/low state (and radio-loud AGN) show a correlation between the x-ray luminosity and radio luminosity (Merloni et al. 2003), which is consistent with radio synchrotron emission from a jet and x-ray emission from a geometrically thick, optically thin, Comptonizing disk.

Some black hole x-ray binaries have jets (Mirabel et al. 1992; Fender 2003), such as GRS 1915+105 with apparently superluminal motion ($\Gamma \sim 3$) (Mirabel & Rodriguez 1994; Mirabel & Rodríguez 1999; Fender & Belloni 2004), but may have $\Gamma \sim 1.5$ (Kaiser et al. 2004). Synchrotron radiation from the jet suggests the presence of a magnetized accretion disk. Observations of a broad, shifted, and asymmetric iron line from GRS 1915+105 is possible evidence for a relativistic accretion disk (Martocchia et al. 2002), although this feature could be produced by a jet component.

The standard paradigm is that relativistic jets from x-ray binaries are probably produced by the Blandford-Znajek effect. However, Gierliński & Done (2004) suggest that at least some black holes, such as GRS 1915+105, have slowly rotating black holes. If this is correct, then another mechanism is required to produce jets. Indeed, jets or outflows are produced from systems containing NSs, young stellar objects, supersoft x-ray white dwarfs, symbiotic white dwarfs, and even UV line-driven outflows from massive O stars. Indeed, a baryon-loaded coronal outflow with $\Gamma \sim 1.5-3$ can be produced from a black hole accretion disk and not require a rapidly rotating black hole (McKinney & Gammie 2004). Nonrelativistic outflows were found even in viscous hydrodynamic simulations (Stone et al. 1999; Igumenshchev & Abramowicz 1999, 2000; McKinney & Gammie 2002). Such baryon-loaded outflows or jets are sufficient to explain most known x-ray binaries without invoking rapidly rotating black holes, and thus unifies such mildly relativistic jets in neutron star and black hole x-ray binaries.

1.3. *AGN*

Active galactic nuclei (AGN) have long been believed to be powered by accretion onto supermassive black holes (Zel'dovich 1964; Salpeter 1964). Observations of MCG 6-30-15 show an iron line feature consistent with emission from a relativistic disk with $v/c \sim 0.2$ (Tanaka et al. 1995; Fabian et al. 2002), although the lack of a temporal correlation between the continuum emission and iron-line emission may suggest it is a jet-related feature (Elvis 2000).

AGN are observed to have jets with $\Gamma \lesssim 10$ (Urry & Padovani 1995; Biretta et al. 1999), even $\Gamma \sim 30$ (Begelman et al. 1994; Ghisellini & Celotti 2001; Jorstad et al. 2001), while some observations imply $\Gamma \lesssim 200$ (Ghisellini et al. 1993; Krawczynski et al. 2002; Konopelko et al. 2003). Some radio-quiet AGN show evidence of weak jets (Ghisellini et al. 2004), which could be explained as a coronal outflow (McKinney & Gammie 2004) and not require a rapidly rotating black hole. Observations imply the existence of a two-component jet structure with a

Poynting jet core and a dissipative surrounding component (Ghisellini & Madau 1996; Ghisellini et al. 2005). The energy structure of the jet and wind are important in understanding the feedback effect that controls size of the black hole and may determine the $M-\sigma$ relation (Springel et al. 2004; Di Matteo et al. 2005).

1.4. *Outline of Paper*

§ 2 summarizes the proposed unified model to explain jet formation in all black hole accretion systems.

§ 3 discusses why ideal MHD must break down in magnetospheres and why the Goldreich-Julian charge density is never reached. A preliminary model is derived that describes the pair-loading and baryon-loading of the Poynting-dominated jet.

§ 4 determines the Lorentz factor of Poynting-dominated jets. The GRB jet Lorentz factor is shown to be based upon electron-positron pair and baryon loading. We show that GRBs likely have electron-proton jets with Lorentz factor at large distances of $100 \lesssim \Gamma_\infty \lesssim 10^3$.

Based upon pair creation rates for AGN and x-ray binaries, we show that relativity low radiatively efficient AGN, such as M87, have electron-positron jets with $2 \lesssim \Gamma_\infty \lesssim 10$. Radiatively efficient systems, such as microquasar GRS1915+105, likely do not have Poynting-dominated lepton jets but rather the observed jets are a relativistic coronal outflow from the inner-disk.

§ 5 discusses Poynting-baryon jets and how they can explain various observational features of jets in AGN and x-ray binaries.

§ 6 summarizes the key results and fits from GRMHD numerical models (McKinney 2005b) used in this paper.

§ 7 discusses the results and their possible implications.

§ 8 summarizes the key points.

Appendix A discusses breakdown of ideal MHD by electron-positron pair creation by radiative annihilation and electron-proton pair creation by ambipolar and Fick diffusion. See also the discussion in McKinney (2005b). Appendix B gives a succinct summary of conserved flow quantities in GRMHD used in section 4. Appendix C gives a derivation for the lab frame stationary GRMHD forces along and perpendicular to the flow (field) line in the lab frame. This elucidates the origin of acceleration and collimation. Appendix D gives the formulae for Comptonization and pair annihilation used in section 4.

2. GRMHD PAIR INJECTION MODEL OF JET FORMATION

The jet energy, composition, collimation, and Lorentz factor are likely determined in a similar way for all black hole accretion systems. The particle acceleration mechanism and particle composition of the jet remained unexplained in McKinney & Gammie (2004). However, if field lines tie the black hole to large distances, then the source of matter is likely pair creation since the amount of matter that diffuses across field lines is much smaller (Phinney 1983; Levinson & Eichler 1993; Punsly 2001). Thus, the Poynting-dominated jet composition is electron-positron pair dominated in AGN and x-ray binaries.

However, in GRB systems, free neutrons lead to baryon contamination due to Fick diffusion across the field lines and subsequent rapid collisionally-induced avalanche decay to an electron-proton plasma (Levinson & Eichler 2003). The pair annihilation rates are much faster than the dynamical time, and due to the temperature decrease, the electron-positron pair rest-mass exponentially drops beyond the fireball formation near the black hole. Thus, the GRB jet composition is likely dominated by electron-proton pairs.

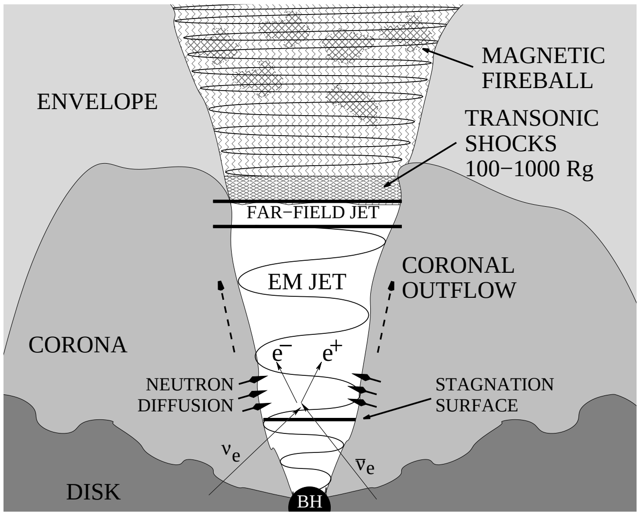

FIG. 1.— Schematic of pair-production model and subsequent magnetic fireball formation for GRB disks. Fireball is extremely optically thick. Below a stagnation surface, pairs are accreted by the black hole and so do not load the jet. Here $Rg = GM/c^2$.

GRMHD numerical models confirmed that accretion of a thick disk with height (H) to radius (R) ratio of $H/R \gtrsim 0.1$ with a homogeneous poloidal orientation self-consistently creates large scale fields that tie the black hole to large distances (McKinney & Gammie 2004; Hirose et al. 2004). Accretion of an irregular field loads the jet with baryons and lowers the speed of the jet. However, the existence of a mostly uniform field threading the disk arises naturally during core-collapse supernovae and NS-BH collision debris disks. In AGN and solar-wind capture x-ray binary systems, the accreted field is probably uniform (Narayan et al. 2003; Uzdensky & Spruit 2005). Roche-lobe overflow x-ray binaries, however, might accrete a quite irregular field geometry. The field geometry that arrives at the black hole, after travelling from the source of material (molecular torus, star(s), etc.) to the black hole horizon, likely depends sensitively on the reconnection physics.

The reason why each system has some observed Lorentz factor has not been well-understood. One key idea of this paper is that the terminal Lorentz factor is determined by the toroidal magnetic energy per unit pair mass density energy near the location where pairs can escape to infinity (beyond the so-called "stagnation surface"). Put another way, the Lorentz factor is determined by the energy flux per unit rest mass flux for the rest-mass flux in pairs beyond the stagnation surface. For GRBs, neutron diffusion is crucial to explain (and limit) the Lorentz factor. For AGN and x-ray binaries, since a negligible number of baryons cross the field lines, pair-loading is crucial to determine the Lorentz factor of the Poynting-dominated jet since this determines the rest-mass flux or density.

Figure 1 shows the basic picture for GRB systems, while figure 2 shows the basic picture for AGN and x-ray binary systems. An accreting, spinning black hole creates a magnetically dominated funnel region around the polar axis. The rotating black hole drives a Poynting flux into the funnel region, where the Poynting flux is associated with the coiling of poloidal magnetic field lines into toroidal magnetic field lines. The accretion disk emits neutrinos in a GRB model (γ-

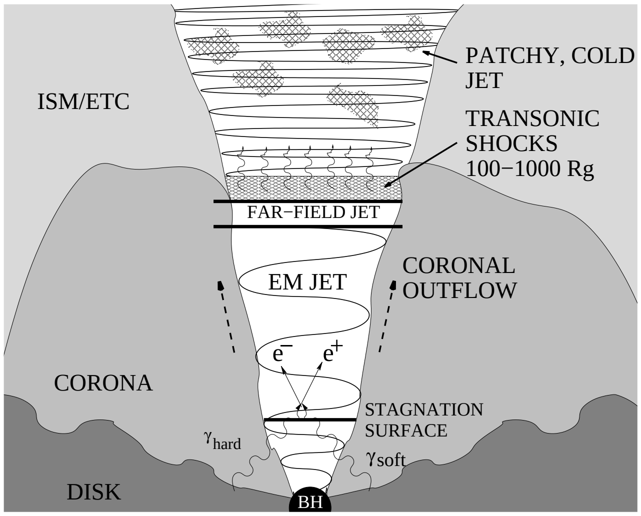

FIG. 2.— Schematic of pair-production model and subsequent shock-heating and emission. AGN jet is optically thin and emits nonthermal and thermal synchrotron, while x-ray binary jet can be marginally optically thick and emit via self-absorbed synchrotron and by severe Compton drag. Severe Compton drag can lead to destruction of the Poynting-dominated jet.

ray and many soft photons for AGN and x-ray binaries) that annihilate and pair-load the funnel region within some "injection region." For GRB systems, neutrons Fick-diffuse across the field lines and collisionally decay into an electron-proton plasma.

Many pairs (any type) are swallowed by the black hole, but some escape if beyond some "stagnation surface," where the time-averaged poloidal velocity is zero and positive beyond. Pairs beyond the stagnation surface are then accelerated by the Poynting flux in a self-consistently generated collimated outflow. In the electromagnetic (EM) jet, the acceleration process corresponds to a gradual uncoiling of the magnetic field and a release of the stored magnetic energy that originated from the spin energy of the black hole.

One key result of this paper is that the release of magnetic energy need not be gradual once the toroidal field dominates the poloidal field, in which case pinch (and perhaps kink) instabilities can occur and lead to a nonlinear coupling (e.g. a shock) that converts Poynting flux into enthalpy flux (Eichler 1993; Begelman 1998). In the proposed GRB model, this conversion reaches equipartition and the jet becomes a "magnetic fireball," where the toroidal field instabilities drive large variations in the jet Lorentz factor and jet luminosity.

In AGN systems, nonthermal synchrotron from shock-accelerated electrons and some thermal synchrotron emission releases the shock energy until the synchrotron cooling times are longer than the jet propagation time. For AGN, jet acceleration is negligible beyond the *extended* shock zone, as suggested for blazars beyond the "blazar zone" (Sikora et al. 2005). In x-ray binary systems, the shock is not as hot and also unlike in the AGN (at least those like M87) case the jet can be optically thick. Thus these x-ray binary systems self-absorbed synchrotron emit if they survive Compton drag.

For all these systems, at large radii patches of energy flux and variations in the Lorentz factor develop due to toroidal instabilities. These patches in the jet could drive internal shocks and at large radii they drive external shocks with the surrounding medium. The EM jet is also surrounded by a mildly relativistic matter coronal outflow/jet/wind, which is a material extension of the corona surrounding the disk. This Poynting-baryon, coronal outflow collimates the outer edge of the Poynting-dominated jet, which otherwise internally collimates by hoop stresses. The luminosity of the Poynting-baryon jet is determined, like the Poynting-dominated jet, by the mass accretion rate, disk thickness, and black hole spin.

This model is studied analytically in this paper, while in a companion paper we study this model numerically using axisymmetric, nonradiative, GRMHD simulations to study the self-consistent process of jet formation from black hole accretion systems (McKinney 2005b). Those simulations extend the work of McKinney & Gammie (2004) by including pair creation (and an effective neutron diffusion for GRB-type systems) to self-consistently treat the creation of jet matter, investigating a larger dynamic range in radius, and presenting a more detailed analysis of the Poynting-dominated jet structure.

Unless explicitly stated, the units in this paper have $GM = c = 1$, which sets the scale of length ($r_g \equiv GM/c^2$) and time ($t_g \equiv GM/c^3$). The mass scale is determined by setting the (model-dependent) observed (or inferred for GRB-type systems) mass accretion rate ($\dot{M}[g\,s^{-1}]$) equal to the accretion rate through the black hole horizon as measured in a simulation. So the mass is scaled by the mass accretion rate at the horizon, such that $\rho_{0,disk} \equiv \dot{M}[r = r_H]t_g/r_g^3$ and the mass scale is then just $m \equiv \rho_{0,disk} r_g^3 = \dot{M}[r = r_H]t_g$. Unless explicitly stated, the magnetic field strength is given in Heaviside-Lorentz units, where the Gaussian unit value is obtained by multiplying the Heaviside-Lorentz value by $\sqrt{4\pi}$.

The value of $\rho_{0,disk}$ can be determined for different systems. For example, a collapsar model with $\dot{M} = 0.1 M_\odot s^{-1}$ and $M \approx 3M_\odot$, then $\rho_{0,disk} \approx 3.4 \times 10^{10}\,\mathrm{g\,cm^{-3}}$. M87 has a mass accretion rate of $\dot{M} \sim 10^{-2} M_\odot\,\mathrm{yr}^{-1}$ and a black hole mass of $M \approx 3 \times 10^9 M_\odot$ (Ho 1999; Reynolds et al. 1996) giving $\rho_{0,disk} \sim 10^{-16}\,\mathrm{g\,cm^{-3}}$. GRS 1915+105 has a mass accretion rate of $\dot{M} \sim 7 \times 10^{-7} M_\odot\,\mathrm{yr}^{-1}$ (Mirabel & Rodriguez 1994; Mirabel & Rodríguez 1999; Fender & Belloni 2004) with a mass of $M \sim 14 M_\odot$ (Greiner et al. 2001), but see Kaiser et al. (2004). This gives $\rho_{0,disk} \sim 3 \times 10^{-4}\,\mathrm{g\,cm^{-3}}$. This disk density scales many of the results of the paper.

3. BREAKDOWN OF IDEAL-MHD

Pair creation is critical to understand the physics of the highly magnetized, evacuated funnel region that is associated with a Poynting-dominated jet. Pair creation is often invoked in order to use the force-free electrodynamics or ideal MHD approximation in a black hole magnetosphere (see, e.g., Blandford & Znajek 1977). However, in MHD where rest-mass is treated explicitly, pair creation is not simply a passive mechanism to short out spark gaps, which is the mechanism invoked to allow the use of the force-free approximation.

Pair creation (and neutron Fick diffusion for GRB-type systems) determines the matter flow in the magnetosphere, and thus the matter-loading of any Poynting jet that emerges (Phinney 1983; Punsly 1991; Levinson 2005). As shown below, these sources of mass loading self-consistently determine the Lorentz factor of the Poynting-dominated jet and allows one to understand why black hole accretion systems, while following the mass-invariant GRMHD equations of motion, show a variety of jet Lorentz factors.

For GRBs, the radiative physics and neutron diffusion is shown to determine the Lorentz factor of the Poynting-dominated jet. For AGN and x-ray binaries, the radiative physics is shown to determine the Lorentz factor of the Poynting-dominated jet by determining its energy and mass-loading.

The ideal MHD approximation (or force-free approximation in magnetically dominated regions) has been shown to be a reasonably valid theoretical framework to describe most of the nonradiative dynamically important accretion physics around a black hole in GRBs, AGN, and black hole x-ray binary systems (Phinney 1983; McKinney 2004). This approximation is the foundation of most studies of jets and winds. The ideal MHD approximation is a good approximation to describe these flow properties except 1) in current sheets, which is not treated explicitly in this paper ; 2) where pair creation contributes a nonnegligible amount of rest-mass, internal energy, or momentum density; 3) if the Goldreich-Julian (GJ) charge density is larger than the number density of charge carriers ; and 4) if the rest-mass flux due to ambipolar and Fick diffusion is negligible.

The first goal is to show that radiative annihilation into pairs establishes a density of pairs much larger than the Goldreich-Julian density. The Goldreich-Julian charge density is never reached because pair creation is completely dominated by neutrino annihilation in GRB-type systems and photon annihilation in AGN and x-ray binary systems.

Notice that the breakdown of ideal MHD is *required* in order to extract black hole spin energy from a stationary, axisymmetric system. Wald (1974) showed that a rotating black hole induces a parallel electric current in the surrounding magnetosphere such that the plasma becomes nondegenerate (i.e. $E^i B_i \neq 0$). Bekenstein & Oron (1978) argued that if the ideal MHD approximation were valid, that no energy could be extracted from a black hole. This is because since $u^r < 0$ at the horizon, and the radial energy flux can be written as $-T^r_t = E\rho u^r$ (where E is conserved along each flow line ; see appendix B), then to extract net energy ($-T^r_t > 0$) from the black hole requires $E < 0$. However, in the ideal MHD approximation $E > 0$ at $r \sim \infty$, and by conservation of E along each flow line, then $E > 0$ on the horizon as well. However, based upon arguments by Goldreich & Julian (1969), Blandford & Znajek (1977) argued that as the magnetosphere is evacuated to the Goldreich-Julian charge density, the parallel electric current separates the charges. The Goldreich-Julian rest-mass density for a species of electrons is

$$\rho_{GJ} \sim m_e \frac{\Omega_H B}{2\pi c q}, \tag{1}$$

where B is the magnetic field strength and q is the electron charge. Once the parallel electric current is sufficiently large, electrons are accelerated across the potential gap and photons can be emitted by curvature radiation or inverse Compton scattering. These high energy photons either self-interact or are involved in a magnetic bremsstrahlung interaction, ultimately leading to electron-positron pairs. These pairs would continuously short the induced potential difference. However, this picture does not establish how the resulting pair plasma flow behaves.

Why have ideal GRMHD numerical models demonstrated the Blandford-Znajek effect (Koide, Shibata, Kudoh, & Meier 2002; McKinney & Gammie 2004; De Villiers et al. 2005a; Komissarov 2005) ? These ideal GRMHD numerical models implicitly break the ideal MHD approximation in the required way to allow the extraction of energy from the black hole. For all the initial conditions and field geometries explored by McKinney & Gammie (2004) using the “ideal” GRMHD numerical model of an accreting black hole, they always find that a highly magnetized polar region forms and any material in this magnetosphere is either rapidly driven into the black hole or driven out in a wind or jet. They find that strong field lines tie the black hole horizon to large radii. Thus, necessarily these ideal MHD models break the ideal MHD approximation at a stagnation point where the poloidal velocity $u^p = 0$. Necessarily matter is created (at least) in this location since matter inside this surface goes into the black hole and matter beyond it goes away from the black hole. This aspect is similar to the charge-starved magnetosphere models where there is a spark-gap (Ruderman & Sutherland 1975) where particles are generated (for a review see Levinson 2005). Once the magnetosphere reaches an axisymmetric, quasi-stationary state, then the departure from the ideal-MHD condition can be measured as deviations from conservation of the conserved flow quantities given in equations B3 to equations B12.

Notice that for a realistic accretion disk the BZ power is different than the typically used estimates (McKinney 2005a). For $j \gtrsim 0.5$, they find that the efficiency in terms of the mass accretion rate is

$$\eta_{EM,tot} = \frac{P_{tot}}{\dot{M}c^2} \approx 15\% \left(\frac{\Omega_H}{\Omega_H[j=1]}\right)^4, \tag{2}$$

and

$$\eta_{EM,jet} = \frac{P_{jet}}{\dot{M}c^2} \approx 7\% \left(\frac{\Omega_H}{\Omega_H[j=1]}\right)^5, \tag{3}$$

where $r_g = GM/c^2$, $\Omega_H = jc/(2r_H)$ is the rotation frequency of the hole, $r_H = r_g(1+\sqrt{1-j^2})$ is the radius of the horizon for angular momentum $J = jGM^2/c$, and $j = a/M$ is the dimensionless Kerr parameter, where $-1 \leq j \leq 1$. However, net electromagnetic energy is not extracted for $j \lesssim 0.5$ (including retrograde accretion) when an accretion disk is present (McKinney & Gammie 2004). This high efficiency is a result of the near equipartition of the magnetic field strength ($(B^r)^2$) in the polar region at the horizon and the rest-mass density in the disk at the horizon. If the black hole has $j \approx 0.9$, then $\approx 1\%$ of the accreted rest-mass energy is emitted back as Poynting flux in the form of a jet and $\approx 3\%$ is emitted back in total (so obviously 2% goes into the disk and corona – about equally it turns out).

3.1. *GRB Pair Creation Model*

In GRB models, such as the collapsar model, neutrino/anti-neutrino annihilation provides a source of electron-positron pairs at a much larger density than the Goldreich-Julian density and so the magnetosphere is not charge starved. The cross-field magnetic diffusion for charged species is negligible in such systems. However, free neutrons diffuse across the field lines and load the jet with an electron-proton plasma (Levinson & Eichler 2003), and this effect is considered in the next section.

For the collapsar model, the jet has $B \sim 3 \times 10^{15}$Gauss (McKinney 2004) and $j \sim 0.9$, which gives

$$\rho_{GJ} \sim 10^{-9} g cm^{-3} \quad \text{(Collapsars)}. \tag{4}$$

One can compare this to the density of pairs produced by neutrino annihilation for the GRB collapsar model. One can use the results in table 3 and figure 9b of Popham et al. (1999) and the results in table 1 in MacFadyen & Woosley (1999), which are fairly well fit to power laws, such that for models with $\dot{M} \leq 0.1 \mathrm{M}_\odot s^{-1}$, and $M = 3\mathrm{M}_\odot$

$$\eta_{\nu\bar{\nu},ann} \equiv \frac{L_{\nu\bar{\nu},ann}}{\dot{M}c^2} \sim 1\% \left(\frac{\alpha}{0.1}\right)\left(\frac{j}{0.9}\right)^7 \left(\frac{\dot{M}}{0.1\mathrm{M}_\odot s^{-1}}\right)^{3.8}, \quad (5)$$

where this fit is based on an average between the conservative and optimistic models of MacFadyen & Woosley (1999). This assumes an average neutrino energy of ~ 10MeV from the disk. This says that for the collapsar model with $j = 0.9$ that about 1% of the rest-mass accreted is given back as positron-electron pairs due to neutrino annihilation, which is similar to the Poynting flux from the black hole that goes into the jet region as from equation 3.

Published results of neutrino annihilation rates as a function of position (Popham et al. 1999) can be used to obtain a preliminary model of pair creation and incorporated into a GRMHD model. The details of this preliminary model end up not affecting the results, and a more self-consistent model is left for future work. The results primarily depend on the overall annihilation luminosity and the basic radial dependence of the energy injected as pairs.

Figure 9 and table 3 in Popham et al. (1999) and table 1 of MacFadyen & Woosley (1999) can be used to obtain approximate radial and height dependent fits of the energy density rate of depositing pairs into the jet region. Their figure 9 shows that the height and radial dependence of the pair annihilation luminosity per unit distance. These follow approximate power laws or exponential laws for $j \gtrsim 0.2$. A reasonable fit is that

$$P[R] \approx e^{-\frac{R-r_g}{2.4r_g}} \quad (6)$$

and

$$Q[z] \approx e^{-\frac{z-r_g}{3.5r_g}} \quad (7)$$

for the luminosity per unit distance. The coefficient is determined by the total annihilation luminosity ($L_{\nu\bar{\nu},ann}$). As in Popham et al. (1999), photon null geodesic transport in curved spacetime is neglected such that

$$L_{\nu\bar{\nu},ann} \sim 2\pi A \int_{r_g}^{\infty} \int_{\theta=0}^{arctan[H/R]} P[R]Q[z]r^2 \sin\theta d\theta dr. \quad (8)$$

Figure 6 of Popham et al. (1999) can be used to obtain the disk thickness to radius ratio

$$H/R \sim 0.1 \left(\frac{r}{2r_g}\right)^{2/3} \quad (9)$$

for $\dot{M} = 0.1\mathrm{M}_\odot s^{-1}$. This allows one to determine that $A \approx L_{\nu\bar{\nu},ann}/191$. Thus the energy generation rate can be written as

$$\frac{\dot{e}_{\nu\bar{\nu},ann}}{\dot{\rho}_{0,disk}c^2} \sim \frac{\eta_{\nu\bar{\nu}}}{N_A} P[R]Q[z] \quad \text{(Collapsars)}, \quad (10)$$

where $N_A \approx 191$ and we have defined $\dot{\rho}_{0,disk} \equiv \dot{M}/r_g^3$. However, the above H/R assumes the jet fills around the disk. Rather, there is likely a thick corona between the disk and jet (McKinney & Gammie 2004). Motivated by those simulations and the simulations discussed in this paper, the jet region is presumed to exist within

$$\theta_j \approx 1.0 \left(\frac{r}{3r_g}\right)^{-1/3} \quad (11)$$

for $r \lesssim 100 r_g$. In that case $N_A \approx 70$. Thus, a significant fraction of the pairs are absorbed by the corona. However, the corona could also *contribute* significantly to neutrino production (Ramirez-Ruiz & Socrates 2005). Thus, $70 \lesssim N_A \lesssim 191$ are reasonable limits.

Some fraction of the total energy deposited goes into pair rest-mass, pair internal energy, radiation, and pair momentum. Here f_ρ denotes the fraction turned into lab-frame mass, f_h the fraction turned into lab-frame internal energy and radiation, and f_m the fraction turned into momentum energy. Thus $1 = f_\rho + f_h + f_m$. The pair rest-mass density creation rate is defined as

$$\frac{\dot{\rho}_{e^-e^+}}{\dot{\rho}_{0,disk}} = f_\rho \frac{\dot{e}_{\nu\bar{\nu},ann}}{\dot{\rho}_{0,disk}}, \quad (12)$$

where $\rho_{e^-e^+} = \rho_{0,e^-e^+} u^t$.

One can obtain a rough density measure in the injection region by assuming the characteristic time scale for moving the pairs once they have formed is the light crossing time at the stagnation surface $t_{stag} \sim t_g(r_{stag}/r_g)$. Then $\rho_{0,e^-e^+} \sim \dot{\rho}_{0,e^-e^+} t_{stag}$. With $\rho_{0,disk} \equiv \dot{\rho}_{0,disk} t_{stag}$,

$$\frac{\rho_{e^-e^+}}{\rho_{0,disk}} \sim f_\rho \left(\frac{\dot{e}_{\nu\bar{\nu},ann}}{\dot{\rho}_{0,disk}c^2}\right)\left(\frac{r_{stag}}{r_g}\right). \quad (13)$$

Notice that many pairs fall into the black hole, so do not contribute to the jet rest-mass or energy. Only those pairs beyond the stagnation surface survive the gravity of the black hole, such that the total annihilation luminosity into the jet is

$$L_{esc} = 2\pi \int_{r=r_{stag}}^{\infty} \int_{\theta=0}^{\theta_j} \dot{e}_{\nu\bar{\nu},ann} r^2 \sin\theta dr d\theta, \quad (14)$$

which is a similar integral as performed before. However, notice that particles injected with $r < r_{stag}$, by definition, fall into the black hole since they are inside the stagnation surface where $u^p < 0$. This is unlike the BZ-power, which in steady state is well-defined and conserved through the stagnation surface (Levinson 2005). For $r_{stag} = r_g$, all the injected mass reaches infinity by definition. For $r_{stag} = 10r_g$, only 11% of the mass injected reach infinity. Because any mass injected lost to the black hole is of no consequence to the acceleration at large distances, then the true efficiency of pairs that load the jet is

$$\eta_{esc} = \frac{L_{esc}}{\dot{M}c^2} \quad (15)$$

rather than $\eta_{\nu\bar{\nu},ann}$ for all r_{stag}. One can show that $\eta_{esc} = \eta_{\nu\bar{\nu},ann}$ for $r_{stag} = r_g$, but is reduced to $\eta_{esc} \approx 0.11\eta_{\nu\bar{\nu},ann}$ for $r_{stag} = 10r_g$ due to the loss of pairs into the black hole.

The pairs annihilate after formed by neutrino annihilation. Equation D7 gives the pair annihilation rate. For GRB models, such as the collapsar model, the pair annihilation timescale is $t_{pa} \sim 10^{-16}$s $\ll GM/c^3 \sim 10^{-5}$s and similarly all along the jet. Thus, the pairs annihilate and form a thermalized fireball. A fraction $f_\rho + f_h$ of the energy injected is turned into a electron-positron pair-radiation fireball. The typical angle of scattering neutrinos gives $f_m \sim f_\rho + f_h$ (Popham et al. 1999). Thus, for the fireball formation region $f_\rho + f_h \sim f_m \sim 0.5$ within factors of a few, and this is independent of the energy of the neutrinos or the efficiency of annihilation.

All of the mass energy thermalizes into the fireball with a temperature given by equation A12. The formation fireball pair mass plus pair internal energy density plus radiation internal energy is

$$\frac{q_{0,tot}u^t u_t + p_{e^-e^+} + p_\gamma}{\rho_{0,disk}c^2} \sim \left(\frac{\dot{e}_{\nu\bar{\nu},ann}}{\dot{\rho}_{0,disk}c^2}\right)\left(\frac{r_{stag}}{r_g}\right), \tag{16}$$

where $q_{0,tot} \equiv (\rho_{0,e^-e^+}c^2 + u_{0,e^-e^+} + u_{0,\gamma})$. This equation connects the energy injection process in terms of the GRMHD equations of motion for a given energy-at-infinity injection rate. See also appendix A.

Using the discussion here and the equations in appendix A, one can show that for $\alpha = 0.1$, $\dot{M} = 0.1 \mathrm{M}_\odot s^{-1}$, and $j = 0.9$, the fireball temperature is $T \sim 10^{10}$K $\sim$ 1MeV in the injection region. Thus pair rest-mass energy is nearly in equipartition with the pair internal energy and radiation. In particular, $f_\rho \approx f_h/8.5$. Since $f_\rho + f_h \sim 0.5$, then $f_\rho \approx 0.05$, $f_h \approx 0.45$, and $f_m \sim 0.5$.

Beyond the initial fireball formation, the Boltzmann factor gives that once the temperature drops below $T \sim 6\times 10^9$K the number of pairs decreases exponentially with temperature. However, the fireball is optically thin only at much larger radii of $r \sim 10^8 - 10^{10} r_g$. So until that radius, the radiation provides an inertial drag on the remaining pair plasma and the gas is radiation dominated.

For example, for $j = 0.9$, $\dot{M} = 0.1\mathrm{M}_\odot s^{-1}$, $r_{stag} = 6r_g$, then the initial fireball rest-mass is

$$\frac{\rho_{e^-e^+}}{\rho_{0,disk}} \sim 10^{-6} \quad (r_{stag} = 6r_g). \tag{17}$$

If instead the model were an $\alpha = 0.01$ model, then the efficiency would be about 10 times less and the density ratio would be about 10 times less at

$$\frac{\rho_{e^-e^+}}{\rho_{0,disk}} \sim 10^{-7} \quad (\alpha = 0.01). \tag{18}$$

In any case this is roughly

$$\rho_{e^-e^+} \gtrsim 10^3 gcm^{-3}, \tag{19}$$

which is about 12 orders of magnitude larger than the GJ density given in equation 4, and so the black hole is far from starved of charges.

3.2. *GRB Baryon Contamination*

Neutron diffusion across field lines leads to baryon contamination of the (otherwise) electron-positron-radiation jet. The neutrons Fick-diffuse (Levinson & Eichler 2003) or diffusion due to ambipolar diffusion (see appendix A) across the field lines and baryon-load the jet. The neutrons undergo a fast collisional avalanche into protons and electrons that are then carried along with the electromagnetic and Compton-thick outflow. As shown in appendix A, the mass injection rate of neutrons (and so proton+electrons) is

$$\dot{M}_{inj,Fick} \sim 7\times 10^{-5}\dot{M}_{acc} \tag{20}$$

where the density of electron-proton plasma is

$$\rho_{pe^-} \sim 3\times 10^{-7}\left(\frac{r}{r_g}\right)^{-4/3}\rho_{0,disk}. \tag{21}$$

Notice that this mass injection rate and density are comparable to the injection-region rest-mass density in electron-positron pairs for $\alpha = 0.01$. As mentioned above, father out in the jet the electron-positron pairs annihilate and contribute only an additional $\sim$ 10% to the internal energy. Thus the total internal energy is sufficient to describe the gas without including pair annihilation and the rest-mass in baryons is sufficient to describe the gas rest-mass for models with $\alpha = 0.01$ and for all models for $r \gtrsim 10r_g$ where the pair-density is exponentially smaller than the baryon density in the jet. Thus, the injection of "pairs" described in the previous section can also approximately account for the Fick diffusion of neutrons. This fact is exploited to simulate the collapsar model in McKinney (2005b).

3.3. *AGN and X-ray Binaries Pair Creation Model*

In AGN and x-ray binaries, the pairs are produced by scattering of $\gtrsim$ 1MeV γ-rays with other photons (for a review see Phinney 1983 and chpt. 6, 9, and 10 in Punsly 2001). These γ-rays could be produced by, for example, Comptonization of disk photons through a gas of relativistic electrons, non-thermal particle acceleration in shocks (see, e.g., Nishikawa et al. 2003), or reconnection events. For example, the (non-radiative) simulations of McKinney & Gammie (2004) show an extended corona that could be source of Comptonization. They also find an edge between the corona and funnel that contains frequent shocks with sound Mach number $M \sim 100$. Also, they found reconnection is quite vigorous in the plunging region at $r \sim 3 - 6r_g$, leading in part to the hot coronal outflow.

These sites of Comptonization, shocks, and reconnection are likely sources of the requisite γ-rays. In place of a detailed model of these processes, it is assumed that some fraction (f_γ) of the true bolometric luminosity is in the form of these γ-rays that do collide with softer photons in the funnel region. For a bolometric luminosity $L_{bol} \sim \eta_{eff}\dot{M}c^2$, then the annihilation efficiency is

$$\eta_{\gamma\gamma,ann} \equiv f_\gamma \frac{L_{bol}}{\dot{M}c^2} = f_\gamma \eta_{eff}, \tag{22}$$

where η_{eff} is the total radiative efficiency, which could include emission from both the disk and jet near the base. Notice that η_{eff} depends on the black hole spin, among other things. However, the value of η_{eff} is obtained from (model-dependent) values for the mass accretion rate and bolometric luminosity.

Extrapolating from gamma-ray observations of black hole x-ray binary systems suggests that in either the quiescent or outburst phase, $f_\gamma \sim 1\%$ of the true bolometric luminosity is in the form of $>$ 1MeV photons (see, e.g., Ling & Wheaton 2005). These are likely produced quite close to the black hole. For an injection region with a half opening angle for the jet of $\theta_j \sim 57^\circ$ (McKinney & Gammie 2004), about $(2\theta_j)^2/(4\pi) \approx 1/3$ of these photons enter the jet region. Thus, it is assumed that a large fraction of these $>$ 1MeV photons give up their energy into producing pairs in the funnel region with some fraction of the energy going into rest-mass (f_ρ). These pairs do not annihilate so form a collisionless plasma (see appendix A). See also Punsly (2001) for why $f_\gamma \sim 1\%$ is reasonable, based on assuming the infall rate is equal to the pair creation rate. In general f_γ depends on the state of the accretion flow, and a self-consistent determination is left for future work.

As in the collapsar case this gives us a density rate or a typical density. In this case the stagnation surface is close to the black hole since the emission is likely always optically thin, thus $r_{stag} = 3r_g$. The author knows of no calculations that give a radial dependence for the annihilation energy generation rate. A reasonable choice is the same radial dependence as for neutrino annihilation, since while the efficiency of neutrino scattering is much lower, the radial structure is determined by a similar calculation. The typical thick disk ADAF model assumes the electrons and protons are weakly coupled, which gives a disk thickness mostly independent of radius such that $H/R \sim 0.85$ and is weakly dependent on α (Narayan & Yi 1995). For the AGN and x-ray binaries, jets are presumed to occur in the presence of a thick (ADAF-like) disk close to the black hole. While observations show that the disk at $r \gtrsim 6r_g$ undergoes state transitions, steady jets are only observed in the low-hard state when the disk is likely geometrically thick. For this H/R, equation 8 gives $A = L_{\gamma\gamma,ann}/53$ or $N_A = 53$. Now equations 12 and 13 also apply for photon annihilation but with $N_A = 53$.

For AGN accretion disks, Phinney (1983) already showed that γ rays from the accretion disk corona interact with x-rays to produce electron-positron pairs in sufficient density above the Goldreich-Julian density. For example, M87 has a nuclear bolometric luminosity of $L_\gamma \approx 2\times 10^{42}\,\mathrm{erg\,s^{-1}}$ and a mass accretion rate of $\dot{M} \sim 10^{-2} M_\odot\,\mathrm{yr}^{-1}$ (Ho 1999; Reynolds et al. 1996) giving $\eta_{eff} \sim 4\times 10^{-3}$. Unlike neutrinos, γ-rays are efficient at creating pairs and most of the γ-rays are at around 1MeV so the fraction of the energy put into rest-mass is $f_\rho \sim 1$. If $f_\gamma \sim 1\%$, then

$$\rho_{e^-e^+} \sim 10^{-23} gcm^{-3} \quad (f_\gamma \sim 1\%). \tag{23}$$

The field strength in M87 is $B \sim 0.1$ to 50Gauss (McKinney 2004). For $j = 0.9$ this gives that

$$\rho_{GJ} \lesssim 10^{-32} gcm^{-3} \quad \text{(M87)}. \tag{24}$$

This is about 9 orders of magnitude lower than the pair creation established density, so the black hole is not charge starved. For M87,

$$\frac{\rho_{e^-e^+}}{\rho_{0,disk}} \sim 10^{-7} \quad \text{(M87)}. \tag{25}$$

For black hole x-ray binaries a similar calculation is performed. For example, GRS 1915+105 has a mass accretion rate of $\dot{M} \sim 7\times 10^{-7} M_\odot\,\mathrm{yr}^{-1}$ and a bolometric luminosity $L \sim 10^{40}\,\mathrm{erg\,s^{-1}}$ (Mirabel & Rodriguez 1994; Mirabel & Rodríguez 1999; Fender & Belloni 2004) with a mass of $M \sim 14 M_\odot$ (Greiner et al. 2001), but see Kaiser et al. (2004). This gives $\eta_{eff} \approx 0.26$. If $f_\gamma \sim 1\%$ and $f_\rho \sim 1$, then

$$\rho_{e^-e^+} \sim 10^{-9} gcm^{-3} \quad (f_\gamma \sim 1\%). \tag{26}$$

The field strength is $B \sim 10^6$Gauss if the disk is in the thick ADAF-like state (McKinney 2004). For $j = 0.9$ this gives that

$$\rho_{GJ} \sim 10^{-19} gcm^{-3} \quad \text{(GRS1915+105)}. \tag{27}$$

This is about 9-10 orders of magnitude larger than the GJ density, so the black hole is not charge starved. For GRS 1915+105,

$$\frac{\rho_{e^-e^+}}{\rho_{0,disk}} \sim 10^{-5} \quad \text{(GRS1915+105)}. \tag{28}$$

Notice that GRS 1915+105, and many x-ray binaries, are more radiatively efficient than most AGN. This means x-ray binaries have jets loaded with more pair-mass density per unit disk density. This will impact the presence and speed of any Poynting-lepton jet, as described in the next section.

Finally, clearly temporal variations in the disk structure and mass accretion rate directly affect the actual pair creation rate in the jet region. A self-consistent treatment of this (time-dependent) radiative physics is left for future work.

4. JET LORENTZ FACTOR

The Lorentz factor of the jet can be measured either as the current time-dependent value, or, using information about the GRMHD system of equations, one can estimate the Lorentz factor at large radii from fluid quantities at small radii. The Lorentz factor as measured by a static observer at infinity is

$$\Gamma \equiv u^{\hat{t}} = u^t\sqrt{-g_{tt}} \tag{29}$$

in Boyer-Lindquist coordinates, where no static observers exist inside the ergosphere. This is as opposed to $W \equiv u^t\sqrt{-1/g^{tt}}$, which is the Lorentz factor as measured by the normal observer as used by most numerical relativists.

For a GRMHD model, to determine the Lorentz factor at $r \sim \infty$, notice that equations B11 and B12 specify that E and L are conserved along each flow line. For flows with a magnetic field that is radially asymptotically small compared to near the black hole, $B_\phi \to 0$ as $r \to \infty$. Also, for a nonradiative fluid, the internal energy is lost to kinetic energy, and so $h \to 1$ as $r \to \infty$. Thus $\Gamma_\infty = -u_t[r=\infty]$. Now, since Φ and Ω_F are conserved along a flow line, then trivially

$$\Gamma_\infty = E = -hu_t + \Phi\Omega_F B_\phi \tag{30}$$

$$u^{\hat{\phi}}_\infty = L = hu_\phi + \Phi B_\phi, \tag{31}$$

where $h = (\rho_0 + u_g + p)/\rho_0$ is the specific enthalpy, Φ is the conserved magnetic flux per unit rest-mass flux, Ω_F is the conserved field rotation frequency, and B_ϕ is the covariant toroidal magnetic field. E and L simply represent the conserved energy and angular momentum flux per unit rest-mass flux. Notice the matter and electromagnetic pieces are separable.

Since E is the hydrodynamic plus magnetic energy flux per unit rest-mass flux, $B_\phi \to 0$ simply represents the conversion of Poynting flux into rest-mass flux and $h \to 1$ represents conversion of thermal energy into rest-mass flux. These are what accelerate the flow. Alternatively stated for the magnetic term, from equation C14, the fluid is accelerated by the magnetic toroidal gradients associated with the Poynting outflow.

A rough estimate of the Lorentz factor at infinity Γ_∞ can be estimated by assuming all the enthalpy flux or all the Poynting flux is lost to rest-mass flux that reach infinity. Then from equation B7, one can break up the matter and electromagnetic numerator and average the numerator and denominator separately to obtain

$$\Gamma_\infty = \Gamma^{(MA)}_\infty + \Gamma^{(EM)}_\infty \sim (\eta_{esc} + \eta_{EM})\left(\frac{\dot{M}_{disk}}{\dot{M}_{esc}}\right), \tag{32}$$

where here "esc" refers to those pairs that escape the black hole gravity. In steady-state, only those pairs beyond the stagnation surface escape to feed the jet.

Before estimating the value of the Lorentz factor for various systems, the toroidal field is shown to be the source of the acceleration in ideal MHD. This also allows a probe of the structure of the jet, which is not possible in the above averages. In ideal-MHD, E and L in equations B11 and B12 give the Lorentz factor at infinity and the angular momentum per particle at infinity.

The enthalpy is just

$$h = (\rho + u + p)/\rho = 1 + \frac{4u}{3\rho} = 1 + \frac{4(1-f_\rho)}{3f_\rho} \tag{33}$$

for a relativistic gas of electron-positron pairs that have f_ρ of energy into rest-mass and the rest into thermal or momentum energy. Now the magnetic term is

$$\Phi\Omega_F B_\phi = \frac{B^\phi B_\phi}{\rho_0 u^t(v^\phi/\Omega_F - 1)}. \tag{34}$$

Notice that E diverges for $v^\phi = \Omega_F$ (or $u^r = u^\theta = 0$), where the ideal MHD approximation breaks down. Thus, Γ_∞ is also determined by the non-ideal MHD physics of particle creation in that region.

For an extended particle creation region, Γ_∞ depends on the mass, enthalpy, and momentum injected as a function of radius and θ in the jet region (Levinson 2005; Punsly 2001). For a narrow ($\delta r \ll r_g$), yet distributed, particle creation region, then plausibly ideal MHD is completely reestablished at a slightly larger radius where $v^\phi \ll \Omega_F \approx \Omega_H/2$ (McKinney & Gammie 2004). In this case $\Phi \approx -\rho\Omega_F u^t/B^\phi$ (or $u^r/B^r \approx -\Omega_F u^t/B^\phi$). Thus, the magnetic piece is

$$\Phi\Omega_F B_\phi \approx \frac{B^\phi B_\phi}{\rho}, \tag{35}$$

where $\rho = \rho_0 u^t$ is the lab-frame density. Written in Boyer-Lindquist coordinates in an orthonormal basis, then the magnetic piece is

$$\Gamma_\infty^{(EM)} \approx \frac{(B^{\hat\phi})^2}{\rho}, \tag{36}$$

where $B^{\hat\phi} = \sqrt{g_{\phi\phi}}B^\phi$. Thus, in Boyer-Lindquist coordinates

$$\Gamma_\infty \sim 1 + \frac{4(1-f_\rho)}{3f_\rho} + \frac{(B^{\hat\phi})^2}{\rho c^2} \tag{37}$$

for $r > r_H$. Thus the fluid energy at infinity is due to conversion of thermal energy and toroidal field energy into kinetic energy. The actual value of Γ_∞ depends on how narrow is the injection region and the location of the stagnation surface. The relevant magnetic field is the toroidal magnetic field strength beyond the injection region where ideal MHD is mostly reestablished. Notice that $\sigma = b^2/\rho_0$ is often used to parameterize the Lorentz factor for a magnetically dominated flow, while perhaps equation 37 is more useful.

The polar field on the black hole horizon is approximately monopolar even for rapidly rotating holes with $j \lesssim 0.95$ (McKinney & Gammie 2004). The monopole field solution can then be used, when properly normalized, to give the functional dependence of $B^{\hat\phi}$ near the black hole. Then one may use equation 37 to obtain the approximate terminal Lorentz factor. First, the black hole emits a Poynting flux given by equation 33 in McKinney & Gammie (2004) with the use of their section 2.3.2 for the magnetic field. In an asymptotic expansion, which is good to factors of 2 for any j even at $r = 3r_g$, then

$$B^{\hat\phi} \approx -C\frac{j}{8r/r_g}\sin\theta. \tag{38}$$

Modifications at higher black hole spin are within factors of 1.5 in magnitude and there is a factor of $\lesssim 1.5$ enhancement near the polar axis compared to lower spin. In order to use this simple BZ monopole, the jet region's "C" coefficient can be obtained from GRMHD numerical models (McKinney & Gammie 2004). For a $H/R \sim 0.2-0.4$ disk model, they find that the normalization constant "C" in the BZ monopole solution is

$$C \approx 0.7\sqrt{\rho_{0,disk}c} \tag{39}$$

(see equations 47-49 in McKinney & Gammie 2004). This clearly states that the toroidal field in the polar region is nearly in equipartition with the rest-mass density in the disk. One can plug this into equation 37, but this equation would have limited usefulness since the injection region is broad and the density is difficult to estimate. However, notice that Γ_∞ has angular structure if the magnetic term dominates since then $\Gamma_\infty \propto \sin^2\theta$. This is important to jet structure described in McKinney (2005b). Otherwise the result has the same qualitative features as equation 46.

4.1. *Lorentz Factors in Collapsar Systems*

This section shows that, without invoking super-efficient neutrino emission mechanisms, only the Blandford-Znajek driven process can drive the flow to the necessary minimal Lorentz factor to avoid the compactness problem and unequivocally generate a GRB. Some GRBs require up to $\Gamma \sim 500$ (Lithwick & Sari 2001), so any invoked mechanism must be able to explain this. Some observation/models suggest some bursts have even $\Gamma \sim 1000$ (Soderberg & Ramirez-Ruiz 2003).

Equation 32 can be written as

$$\Gamma_\infty = \left(\eta_{esc} + \eta_{EM,jet}\right)\left(\frac{\dot M}{\dot M_{esc}}\right). \tag{40}$$

Equation 15 gives η_{esc}, which accounts for pair capture by the black hole. Here η_{EM} is given in equation 3 and as generally noted before, $\eta_{esc} = \eta_{\nu\bar\nu,ann}$ for $r_{stag} = r_g$, but is reduced to $\eta_{esc} \approx 0.11\eta_{\nu\bar\nu,ann}$ for $r_{stag} = 10r_g$ due to the loss of pairs into the black hole. Based upon GRMHD numerical models studied in McKinney (2005b), a likely value is $r_{stag} = 5r_g$, for which $\eta_{esc} \approx 0.5\eta_{\nu\bar\nu,ann}$.

GRB-type systems are different than AGN and x-ray binary systems, because neutron diffusion baryon-loads the jet. The indirect injection of protons and electrons is shown to dominate the rest-mass in the jet because the electron-positron pairs annihilate to negligible rest-mass. The Fick diffusion mass injection rate is given by equation A10 and is

$$\dot M_{inj,Fick} \sim 7\times 10^{-5}\dot M_{acc} \tag{41}$$

(Levinson & Eichler 2003), and so $\dot M_{esc} = \dot M_{inj,Fick}$.

Plugging in the efficiencies for neutrino annihilation (equation 5) and Poynting-dominated jet efficiency (equation 3) into equation 40, one finds for $\dot M \leq 0.1 M_\odot s^{-1}$ for $j \gtrsim 0.1$ that

$$\Gamma_\infty \sim 140\left(g_{\nu\bar\nu,ann,esc} + g_{EM,jet}\right) \tag{42}$$

where

$$g_{\nu\bar\nu,ann,esc} \equiv \left(\frac{\eta_{esc}}{\eta_{\nu\bar\nu,ann}}\right)\left(\frac{\alpha}{0.1}\right)\left(\frac{j}{0.9}\right)^7\left(\frac{\dot M}{0.1 M_\odot s^{-1}}\right)^{3.8} \tag{43}$$

where for $\dot M \gtrsim 0.1 M_\odot s^{-1}$, the power of 3.8 sharply levels out to 0 (Di Matteo et al. 2002). Also,

$$g_{EM,jet} \equiv 7\left(\frac{j}{1+\sqrt{1-j^2)}}\right)^5. \tag{44}$$

These g's are just the normalized the efficiencies. It turns out that for $j \approx 0.9$ that the efficiencies are similar for the shown normalization of parameters. Thus, one might expect that they contribute equally to the energy of the jet.

If $r_{stag} = r_g$ and $\alpha = 0.1$, then for the collapsar model with $\dot M = 0.1 M_\odot s^{-1}$ and $j = 0.9$, then neutrino annihilation and BZ power are equal and typically give $\Gamma \sim 100-140$, which is sufficient to avoid the compactness problem for typical bursts.

However, $r_{stag} \approx 5r_g$ is more likely. The neutrino-driven term then gives $\Gamma_\infty \sim 70$ and is dominated by the BZ-driven term that stays at $\Gamma_\infty \sim 100$. This is a result of the loss of pairs into the black hole. Notice that the results of (Popham et al. 1999; Di Matteo et al. 2002) and others do not include Kerr geometry to trace null geodesics. While the efficiency for annihilation should increase due to gravitational focusing, more pairs are also absorbed by the black hole. Thus, it is unlikely that gravitational focusing helps the neutrino-driven mechanism.

Also, $\alpha = 0.1$ probably considerably overestimates the viscous dissipation rate of a true MHD flow. Despite typically $\alpha = 0.1$ being used by many authors studying viscous models of disks, Stone & Pringle (2001) showed that $\alpha = 0.01$ is more representative of MHD disks near the black hole. This implies that the energy generation rate in the disk and the generation rate of neutrinos is lower by about an order of magnitude. For normal neutrinos this gives $\Gamma_\infty \sim 14$, insufficient to explain GRBs.

Another problem for the neutrino annihilation mechanism is that, with the inclusion of optically thick neutrino transport, the efficiency of neutrino emission is another few times lower for the collapsar model (Di Matteo et al. 2002). This gives $\Gamma_\infty \sim 5$, clearly a serious problem for the neutrino annihilation model of GRBs.

The annihilation efficiency approximately scales with the average neutrino energy (Popham et al. 1999). One must invoke super-efficient neutrinos with an average neutrino energy of ~ 210MeV (Ramirez-Ruiz & Socrates 2005) in order to obtain a neutrino annihilation power comparable to the BZ power. However, this is near the peak neutrino energy estimated to come from a hot corona (Ramirez-Ruiz & Socrates 2005), and the corona is not expected to be the dominant source of neutrinos, so the average neutrino energy should be smaller.

Notice that choosing $j = 1$ only increases the neutrino efficiency, and so Γ_∞, by a factor of 2. Such a black hole spin is only achievable when $H/R \lesssim 0.01$ (Gammie, Shapiro, & McKinney 2004), which is not representative of any GRB model (Kohri et al. 2005).

So, without evoking super-efficient neutrino emission mechanisms and unreasonably large neutrino annihilation efficiencies based upon only optically thin emission, one must turn to the Poynting flux to drive the jet. For $j = 0.9$ one has $\Gamma_\infty \sim 100$, sufficient to avoid the compactness problem is many GRBs and only invokes an obtainable black hole spin. Unlike the neutrino annihilation case, the BZ efficiency has been computed self-consistently from GRMHD numerical models of GRB-type disks (McKinney 2005b).

Just as the neutrino-case has a proposed super-efficient mechanism, there are super-efficient magnetic models that would increase the terminal Lorentz factor. Eventually after accreting a large amount of magnetic flux, the magnetic pressure dominates the ram pressure of the accretion flow and suspends the flow (Igumenshchev et al. 2003; Narayan et al. 2003). GRMHD numerical models are suggested to not have simulated for long enough to see this effect. In this case a larger amount of magnetic flux threads the black hole. In this magnetically arrested disk (MAD) model, the field strength is *comparable* to the rest-mass density in this case rather than only a fraction of it. Then, the BZ efficiency is 100% for $j = 1$ and an estimate of the jet efficiency is about 50%, which is ~ 10 times larger than previously. Thus potentially $\Gamma \sim 1000$ is achievable with $j = 0.9$. Only super-efficient neutrinos with average energy 2100MeV can obtain such a jet power.

At the moment there is an insufficient study of the neutrino annihilation rates for disks that have large optically thick regions, so Γ_∞ is not directly estimated for BH-NS or NS-NS collisions. However, at higher mass accretion rates the neutrino emission efficiency levels off rather than increasing (Di Matteo et al. 2002), suggesting these systems should also be dominated by Poynting-flux energy like for collapsars.

In summary, the neutrino-driven mechanism is probably dominated by the BZ power. Corrections due to optically thick neutrino-transport, a realistic choice for α based upon MHD models, and the loss of pairs into the black hole are the primary reducing factors compared to previous expectations. However, the BZ-effect generates sufficiently energetic GRBs while only invoking an obtainable black hole spin.

Also, while a hydrodynamic jet mixes and can destroy jet structure, an electromagnetic jet can internally evolve and could have a distribution of Lorentz factors in the jet. This is what is found in McKinney (2005b). Thus, while the electromagnetic jet may on average have $\Gamma \sim 100$, the core of the jet may have $\Gamma \sim 1000$. Thus, without invoking super-efficient mechanisms, only an electromagnetic BZ-driven jet can explain all observed/inferred GRB Lorentz factors.

Based upon the density scaling from the simulations in McKinney (2005b) that are summarized in section 6.2, and based upon appendix D, the fireball is optically thick to Compton scattering until $r \sim 10^8 - 10^{10} r_g$. Simulations discussed in McKinney (2005b) show that Poynting flux is continuously converted to heat in shocks and so all the energy flux leads to acceleration. Thermal acceleration occurs until the fireball is optically thin. This acceleration reaches $\Gamma \sim 100-1000$ before the internal shocks generate the non-thermal emission.

4.2. *Lorentz Factors in AGN and X-ray Binary Systems*

This section shows that the *disk+jet* radiative physics is crucial to determine the Lorenz factor of jets. It is shown that radiatively inefficient AGN, such as M87, should have jets with $2 \lesssim \Gamma \lesssim 10$, while radiatively efficient systems, such as GRS 1915+105, may have jets with $\Gamma \lesssim 2$, but they may be Compton dragged to *nonrelativistic* velocities.

For AGN and x-ray binaries equation 32 can be written as

$$\Gamma_\infty = \frac{1}{f_\rho}(\eta_{esc} + \eta_{EM})\left(\frac{\dot{M}c^2}{L_{esc}}\right), \tag{45}$$

for a fraction $\dot{M}_{esc} = f_\rho L_{esc}$ of mass that escapes the gravity of the hole. Equation 15 shows that the mass-energy loading of the jet is reduced, compared to the total injected mass-energy, due to loss of pairs into the black hole. Since $\eta_{esc} \equiv L_{esc}/(\dot{M}c^2)$, then

$$\Gamma_\infty \sim \frac{1}{f_\rho}\left(1 + \frac{\eta_{EM}}{\eta_{esc}}\right) \tag{46}$$

Here η_{EM} is given in equation 3. As noted before, $\eta_{esc} = \eta_{\gamma\gamma,ann}$ for $r_{stag} = r_g$, but is reduced to $\eta_{esc} \approx 0.11\eta_{\gamma\gamma,ann}$ for $r_{stag} = 10r_g$ due to the loss of pairs into the black hole.

For these systems $r_{stag} \approx 3r_g$, since the disk is likely optically thin and emits harder radiation closer to the black hole. This gives $\eta_{pairs}/\eta_{ann} \sim 0.83$ for the ADAF model of H/R. Here the fraction of energy in rest-mass is $f_\rho \sim 1$ due to the efficiency of photon-photon annihilation for > 1MeV photons off the plentiful softer photons. As discussed before, observations suggest that the fraction of bolometric luminosity in γ-rays is $f_\gamma \sim 0.01$. Since the radiative efficiency should also depend on black hole spin, it is assumed a typical system has $j \sim 0.9$ since that is a plausible equilibrium spin (Gammie, Shapiro, & McKinney 2004). A detailed model of the radiative efficiency as a function of black hole spin is left for future work.

Equation 46 then gives that

$$\Gamma_\infty \sim 1 + \left(\eta_{eff}\right)^{-1}. \tag{47}$$

For M87, $\eta_{eff} = 0.004$ so $\Gamma_\infty = 250$, while for GRS1915+105 $\eta_{eff} = 0.26$ so $\Gamma_\infty = 5$.

As cited in the introduction, the observed apparent Lorentz factor of AGN jets is $\Gamma_\infty \lesssim 30$, while inferred Lorentz factor of some AGN jets is $\Gamma_\infty \lesssim 200$, in basic agreement with the above estimates. However, in particular for M87 this is rather large. Also, the GRS1915+105 estimate is a bit large.

The key difference between the collapsar event and AGN or x-ray binaries is that in the collapsar case the photon luminosity (including Compton upscattered by Γ^2) is negligible compared to the jet luminosity, but see Ghisellini et al. (2000); Lazzati et al. (2004). In M87 the bolometric luminosity L_{bol} is almost that of the jet luminosity P_{jet}. In GRS 1915+105 the bolometric luminosity is *greater* than the jet luminosity.

The below discussion is a preliminary check on how radiative processes affect the above results. The results of simulations from McKinney (2005b) are invoked in order to obtain the density and magnetic structure of the Poynting-lepton jet as summarized in section 6.2. The simulations also show that at $r \sim 10^2 - 10^4 r_g$, any remaining Poynting flux is shock-converted into enthalpy flux until they are in equipartition. A self-consistent simulation with synchrotron emission would then show the continuous loss of Poynting flux until the synchrotron cooling timescale is longer than the jet propagation timescale. This still suggests the jet magnetic field is finally in equipartition, but that much of the energy is lost and so cannot acceleration the jet.

The *jet*, rather than just disk, radiative physics is necessary in order to explain why $\Gamma_\infty = 250$ is not achieved in M87 and $\Gamma_\infty = 5$ is not achieved in GRS 1915+105. For M87, much of the Poynting energy that leads to $\Gamma_\infty \sim 250$ is converted to heat by shocks, which is then lost to nonthermal and some thermal synchrotron emission. Thus the Lorentz factor of the Poynting-lepton jet achieved by $r \sim 10^2 - 10^3 r_g$ is likely the maximum obtainable. Numerical models of M87 discussed in McKinney (2005b) show that $2 \lesssim \Gamma \lesssim 10$. The Poynting-lepton jet in GRS 1915+105 is likely destroyed by Compton drag or at best $\Gamma_\infty \lesssim 2$. Other black hole accretion systems with different mass accretion rates and radiative efficiencies have to be independently checked. The below discussion of the disk+jet radiative physics should be considered preliminary since a full radiative transport is necessary to obtain a completely self-consistent solution.

4.2.1. *Jet Destruction by Bulk Comptonization*

The previous section showed that jets from AGN and x-ray binaries survive loading by pair production from γ-ray photons, but the produced jet may not survive Compton drag (bulk Comptonization) by the relatively soft photons emitted by the disk.

The simulation-based results are used to determine the optical depth as given in equations D3 and D5 to compute the perpendicular and parallel optical depths to Comptonization. For M87 $\tau_{\|} \sim 6\times10^{-6}$ and $\tau_\perp \sim 6\times10^{-6}$ at $r \sim 5r_g$ (stagnation surface where jet starts) and $\tau_\perp \sim 4\times10^{-6}$ at $r = 120 r_g$. For GRS 1915+105, $\tau_{\|} \gtrsim 11$ and $\tau_\perp \lesssim 4$ (stagnation surface) and $\tau_\perp \lesssim 3$ at $r = 120 r_g$. Thus M87 is not Compton dragged by the disk photons, while GRS 1915+105 is likely strongly Compton dragged by photons that originate near the base of the jet and travel up through the jet or across the jet, or by synchrotron self-Compton drag.

A Compton-dragged jet has a limited Lorentz factor that reaches an equilibrium between decelerating and accelerating radiative processes. Here is it assumed that most of the disk emission is at the base of the jet. Then the relevant scenario for GRS 1915+105 is the one where all disk seed photons that enter the jet are scattered. An isotropic disk luminosity L_{bol} shining on a conical jet with half-opening angle θ_j dumps a luminosity of $L_{seed} \sim \theta_j^2 L_{bol}/4$ into the jet. The photons effectively mass-load the jet and an equilibrium Lorentz factor is reached, where

$$\Gamma_\infty \sim \left(\frac{P_{jet}}{2L_{seed}}\right)^{1/3} \sim \left(\frac{2\eta_{EM,jet}}{\eta_{eff}\theta_j^2}\right)^{1/3} \tag{48}$$

for a cold beam of electrons (see, e.g., Broderick 2004). The thermal Lorentz factor is comparable to the bulk Lorentz factor, so thermal corrections are not significant. For GRS 1915+105 this gives a *nonrelativistic* velocity ($\Gamma \sim 1$) for the jet if most of the emission enters the base. Only if most of the emission enters far ($r \gtrsim 10^2 r_g$) from the base is up to $\Gamma \sim 2$ possible. Thus is unlikely, so the Poynting-lepton jet that forms in radiatively efficient systems, such as GRS 1915+105, are Compton dragged to *nonrelativistic* velocities. Clearly the Lorentz factor is sensitive to the disk thickness, the emission from the disk, and the structure of the jet. Thus these estimates should be treated as preliminary. A self-consistent radiative transfer calculation is left for future work.

In summary, a radiatively efficient system loads the jet with more pairs from the larger number of γ-rays. This sets the maximum possible Lorentz factor to be smaller than for radiatively inefficient systems. For systems with relatively high density jets, such as X-ray binaries, the larger radiative efficiency also leads to an optically thick jet that can be Compton dragged.

4.2.2. *Jet Destruction by Pair Annihilation*

Equation D7 gives the pair annihilation rate. For AGN, such as M87, the pair annihilation timescale is $t_{pa} \sim 10^{11}$s $\gg GM/c^3 \sim 10^4$s and for a jet propagation time $t_{jet} \sim r/c$, a lower limit is $t_{pa}/t_{jet} \gtrsim 10^7$ all along the jet. Thus, most pairs do not annihilate. See appendix A on how this affects the fluid approximation. See also Ghisellini et al. (1992).

For X-ray binary GRS1915+105, $t_{pa} \sim 2\times10^{-4}$s $\gtrsim GM/c^3 \sim 7\times10^{-5}$s and $t_{pa}/t_{jet} \gtrsim 2$ all along the jet. Thus, some nonnegligible fraction of the pairs annihilate. This also contributes to the destruction of the Poynting-lepton jet in X-ray binary systems since much of this radiative energy is lost at $r \gtrsim 150 r_g$ where the jet is optically thin along the jet and $r \gtrsim 300 r_g$ where the jet is optically thin perpendicular to the jet.

4.2.3. *Heat Loss by Synchrotron Emission*

For M87 it was estimated that $\Gamma_\infty \sim 250$, which is inconsistent with observations. However, much of the Poynting energy is converted to internal energy in shocks induced by toroidal field instabilities (McKinney 2005b). Thus, the synchrotron cooling time might be sufficiently fast to release this internal energy that would otherwise accelerate the flow through thermal acceleration. For numerical models described in McKinney (2005b) that correspond to M87, an equipartition "magnetic fireball" forms between $10^2 r_g$ and $10^3 r_g$. If this energy could be released, then the shocks would again resume and all the Poynting and thermal energy would be lost. For an equipartition magnetic fireball half the energy is thermal, so the jet internal energy is $u_{e^-e^+} \sim 125\rho_{0,e^-e^+}c^2$ and so the thermal Lorentz factor is $\Gamma_e \sim 125$. The synchrotron cooling time in the lab frame is

$$t_{syn} \sim \frac{\Gamma_{bulk}\Gamma_e m_e c^2}{P_{syn}} \sim 6\pi \frac{\Gamma_{bulk} m_e c^2}{\Gamma_e \sigma_T c B^2}. \qquad (49)$$

This gives that

$$t_{syn} \sim 10^4 s \left(\frac{r}{r_g}\right)^{1.4} \quad (r < 390 r_g, \mathrm{M87}) \qquad (50)$$

and

$$t_{syn} \sim 1 s \left(\frac{r}{r_g}\right)^{3} \quad (r > 390 r_g, \mathrm{M87}). \qquad (51)$$

For a typical lab frame jet propagation time of $t_{jet} \sim r/c$,

$$\frac{t_{syn}}{t_{jet}} \sim \left(\frac{r}{r_g}\right)^{0.4} \quad (r < 390 r_g, \mathrm{M87}) \qquad (52)$$

and

$$\frac{t_{syn}}{t_{jet}} \sim 10^{-4} \left(\frac{r}{r_g}\right)^{2} \quad (r > 390 r_g, \mathrm{M87}). \qquad (53)$$

Hence, one would *not* expect synchrotron cooling to take much of the internal energy away.

However, the "magnetic fireball" forms by shock heating and electrons are dramatically accelerated in such relativistic collisionless shocks. The shocks generate a power law (nonthermal) distribution of electrons, where much of the energy is carried by high-energy electrons (Begelman et al. 1984; Blandford & Eichler 1987; Achterberg et al. 2001; Fender & Maccarone 2003; Keshet & Waxman 2005; Fender et al. 2005). Typically the distribution is $N(E) \propto E^{-2.22}$. For a pair plasma the maximum energy is limited by synchrotron losses (Achterberg et al. 2001), and the resulting synchrotron emission has photon energies of $E \sim 25\Gamma_e$MeV. This gives γ-ray and up to possibly TeV emission beamed along the jet, as in blazars. For example, Mrk 421 shows 15 minute variability, which for a mass of $1.9 \times 10^8 M_\odot$ would suggest an emission size on the order of the horizon size (Punch et al. 1992; Gaidos et al. 1996). However, relativistic time effects with $\Gamma_{bulk} \sim 10$ place these emissions at $r \sim 10^2 r_g$, which coincides with the shock-heated transfast region discussed in (McKinney 2005b).

Thus, a significant portion of the shock-heated internal energy should be emitted by shock accelerated electrons and lost through the optically thin jet. In the shocks, inverse Compton also contributes to emission of high-energy photons and the loss of internal energy. Shock-induced population inversions may generate cyclotron masers at shock sites and lead to large brightness temperatures (Begelman et al. 2005).

Thus, it is expected that much of the jet is cold with $\Gamma_{bulk} \sim 5-10$ left over from pre-shock magnetic acceleration. As described in the simulations of McKinney (2005b), patches of slightly faster or slower bulk Γ are present by $r \sim 10^2 r_g$. In M87-based models, these range from $2 \lesssim \Gamma \lesssim 10$.

The synchrotron emission angular frequency is

$$\omega_c \sim \frac{3\Gamma_e^2 qB \sin\alpha}{2m_e c}, \qquad (54)$$

where $\sin\alpha \sim 1$. This gives a characteristic synchrotron frequency of

$$\nu_c \sim 3 \times 10^{12} \left(\frac{r}{r_g}\right)^{-0.7} \mathrm{Hz} \quad (r < 390 r_g, \mathrm{M87}) \qquad (55)$$

and

$$\nu_c \sim 3 \times 10^{14} \left(\frac{r}{r_g}\right)^{-1.5} \mathrm{Hz} \quad (r < 390 r_g, \mathrm{M87}). \qquad (56)$$

For $r \sim 10^2 r_g$ where the fireball begins to form, this gives $\nu_c \sim 100$GHz (radio). By $r \sim 10^3 r_g$, $\nu_c \sim 10$GHz (radio). The emission frequency depends on the mass accretion rate (and so $\rho_{0,disk}$) for any particular AGN. As discussed in McKinney (2005b), $r \sim 10^2 r_g$ is also where the flow goes superfast (supersonic). Thus this is consistent with the idea that the radio-bright static knots at the base of the jet in, for example, Cen A is due to shocks in a transfast (transonic) transition (Hardcastle 2005).

In summary, the jet in M87 likely emits most of the internal energy, generated in shocks in the transonic transition, as nonthermal synchrotron with some thermal synchrotron, such that the jet beyond $10^3 - 10^4 r_g$ is relatively cold with $2 \lesssim \Gamma_\infty \lesssim 10$.

Notice that in x-ray binaries, for example GRS 1915+105, have a jet with $u/\rho_{0,e^-e^+}c^2 \sim 2.5$ and so thermal $\Gamma_e \sim 2.5$. This gives that

$$t_{syn} \sim 10^{-7} \mathrm{s} \left(\frac{r}{r_g}\right)^{1.4} \quad (r < 390 r_g, \mathrm{GRS}) \qquad (57)$$

and

$$t_{syn} \sim 10^{-11} \mathrm{s} \left(\frac{r}{r_g}\right)^{3} \quad (r > 390 r_g, \mathrm{GRS}). \qquad (58)$$

For a typical lab frame jet propagation time of $t_{jet} \sim r/c$,

$$\frac{t_{syn}}{t_{jet}} \sim 10^{-3} \left(\frac{r}{r_g}\right)^{0.4} \quad (r < 390 r_g, \mathrm{GRS}) \qquad (59)$$

$$\frac{t_{syn}}{t_{jet}} \sim 10^{-7} \left(\frac{r}{r_g}\right)^{2} \quad (r > 390 r_g, \mathrm{GRS}), \qquad (60)$$

where GRS denotes GRS1915+105. Thus thermal synchrotron is sufficiently fast to cool the jet. Since the jet is optically thick, as estimated above, then synchrotron self-absorption will dominate the emission process, which is what is observed (Foster et al. 1996; Fender & Belloni 2004). The thermal synchrotron emission has

$$\nu_c \sim 2 \times 10^{15} \left(\frac{r}{r_g}\right)^{-0.7} \mathrm{Hz} \quad (r < 390 r_g, \mathrm{GRS}) \qquad (61)$$

and

$$\nu_c \sim 3 \times 10^{17} \left(\frac{r}{r_g}\right)^{-1.5} \mathrm{Hz} \quad (r > 390 r_g, \mathrm{GRS}). \qquad (62)$$

Near the base this gives 0.01keV emission (EUV). These soft synchrotron photons will be Compton upscattered (synchrotron self-Compton) by the $\Gamma \lesssim 5$ jet to x-rays and contribute to the destruction of the Poynting-lepton jet. Like in AGN, nonthermal synchrotron likely takes away much of the shock-generated internal energy and this may account for some unidentified EGRET sources.

It is beyond the scope of the present study to establish whether nonthermal synchrotron, synchrotron self-Compton, or external Comptonization accounts for most of the high-energy luminosity.

4.2.4. *Other issues*

Another possible way of contaminating the Poynting-dominated jet is by accreting a complicated field geometry and so baryon-loading the polar region. This turns the jet into a mixed lepton-baryon Poynting jet. Core-collapse presents the black hole with a field geometry that has an overall single poloidal sign. Compared to GRBs, AGN and x-ray binary black holes are more likely to accrete nontrivial field geometries leading to baryon contamination of the jet. Especially in Roche-lobe formed disks in x-ray binaries, it is likely that the accreted field geometry is quite tangled, so the likelihood of a relativistic Poynting jet is further reduced.

No black hole x-ray binary has been observed to have an ultrarelativistic jet (V4641 Sgr is still not confirmed, but see Chaty et al. 2003), despite the GRMHD physics in such systems being identical and the Lorentz factor is otherwise independent of the mass of the compact object. However, due to their relatively high radiative efficiency compared to AGN, x-ray binaries produce more γ-ray flux that increases the pair loading for a given magnetic field strength near the black hole. Also, the relatively high radiative efficiency means any Poynting-lepton jet is severely Compton dragged since the jet is optically thick. However, it is possible that there exists a large population of low radiative efficiency galactic black hole accretion systems. These radiatively inefficient systems would produce a large amount of Poynting flux per unit rest-mass flux which would be shock-converted by toroidal field instabilities into nonthermal synchrotron emission and could appear as "microblazars." However, thus-far observed x-ray binaries should not be as intrinsically luminous per rest-mass accretion rate since the Poynting flux per rest-mass flux available to shock-heating is two orders of magnitude smaller than available for AGN. This is due to the relatively high pair-loading in typical x-ray binaries. Low-luminosity x-ray binaries would behave more like blazars, and so low luminosity x-ray binary microblazars may account for some of the unidentified EGRET sources.

5. RELATIVISTIC POYNTING-BARYON JETS

This section discusses how mildly relativistic Poynting-baryon jets can explain many jet observations. The origin of these jets is the inner-radial accretion disk. The origin of the mass is unstable convective outflows and magnetic buoyancy, and the mass fraction released is typically a few percent of the mass accretion rate (McKinney & Gammie 2004; De Villiers et al. 2005a). The ratio of Poynting to baryon flux depends mostly on the spin of the black hole (Punsly & Coroniti 1990a,b; McKinney & Gammie 2004). Since the Poynting flux from a rapidly rotating black hole that is absorbed by the corona is also a few percent, the Poynting-baryon jet is heavily baryon-loaded. The heavy baryon-loading limits Poynting-baryon jets to only mildly relativistic velocities. The most relativistic, collimated, and least baryon-loaded portion of the Poynting-baryon jet is at the magnetic wall bounded by the Poynting-dominated jet.

5.1. *Matter Jets and Outflows in AGN*

Most AGN should have Poynting-baryon jets. This Poynting-baryon jet may often lead to erroneous conclusions about the nature of the jet in AGN systems.

For example, Junor et al. (1999); Biretta et al. (1999, 2002) suggest that M87 slowly collimates from about 60° near the black hole to 10° at large distances. However, two of their assumptions are likely too restrictive. First, they assumed the jet is always conical, which is apparent from figure 1 in Junor et al. (1999). If the jet is not conical this can overestimate the opening angle close to the core (i.e. perhaps 35° is reasonable all the way into the core). Second, their beam size is relatively large so that factors of 2 error in the collimation angle are likely. Finally, and most importantly for this paper, they assumed that there is only one jet component. This likely leads to a poor interpretation of the observations. If there is a highly collimated relativistic Poynting-lepton jet surrounded by a weakly collimated Poynting-baryon jet, then this would also fit their observations.

Alternatively, if the accretion disk in M87 is a very thin SS-type disk with $H/R \sim 0.00048$ (McKinney 2004), then their conclusion that there is slow collimation is plausible. However, thin disks may be much less efficient at producing jets (Livio, Ogilvie, & Pringle 1999; Ghosh & Abramowicz 1997) and may not be able to produce collimated jets (Okamoto 1999, 2000). A form of the idea that winds collimate jets has also been proposed by Tsinganos & Bogovalov (2005) and applied to M87, but they consider a model where the wind slowly collimates the jet in order to fit observations. Here we suggest that the observations have been misinterpreted due to the presence of two components: a well-collimated relativistic cold Poynting-lepton jet and a mildly relativistic coronal outflow. We suggest the broader emission component is due to the coronal outflow.

Notice that more recent maps of the M87 jet-formation region show no "jet formation" structure (Krichbaum et al. 2004). Thus, the structures seen previously may be transient features, such as associated with turbulent accretion disk producing a dynamic coronal outflow.

Measurements of the apparent jet speed in M87 reveal typically $\Gamma \sim 1.8$ near the core while $\Gamma \sim 6$ at larger radii. However, some core regions are associated with $\Gamma \sim 6$ that rapidly fade (Biretta et al. 1999). This is consistent with a two-component outflow where the cold fast moving core of the jet is only observed if it interacts with the surrounding medium (or stars), the slower coronal outflow, or it undergoes internal shocks.

For relatively thin disks or slowly rotating black holes, Poynting-baryon jets could appear as "aborted jets" (Ghisellini et al. 2004).

The classical AGN unification models (Urry & Padovani 1995) invoke a dominant role for the molecular torus and broad-line emitting clouds, while the broad coronal outflow may significantly contribute to modifications and in understanding the origin of the clouds (Elvis 2000; Elvis et al. 2004).

Other erroneous conclusions could be drawn regarding the jet composition. Entrainment, which could occur at large distances when the ideal MHD approximation breaks down, causes difficulties in isolating the "proper" jet component's composition. Worse is the fact that there should be two separate relativistic jet components, making it difficult to draw clear conclusions regarding the composition (Guilbert et al.

1983; Celotti & Fabian 1993; Levinson & Blandford 1996; Sikora & Madejski 2000). However, is has been recently suggested that only electron-positron jets could explain FRII sources (Kino & Takahara 2004).

It is also often assumed that if the jet is highly collimated that it is also highly relativistic near the black hole, which would suggest Comptonization of disk photons should produce clear spectral features (Sikora & Madejski 2000). However, the jet may rather slowly accelerate and quickly collimate, which is universally what GRMHD numerical models find.

5.2. *Jets in X-ray Binaries*

The results of the previous section suggest that the term "microquasar" does not accurately reflect the jet formation process. If radiatively efficient systems have no Poynting-lepton jet, then what produces their jets? Mildly relativistic jets from black hole microquasars may be produced by the inner-radial disk rather directly by the black hole. The above results suggest that GRS1915+105 may not have a Poynting-lepton jet during its quiescent accretion phase in the low-hard state. All black hole accretion systems with a thick disk have a mildly relativistic $1 \lesssim \Gamma \lesssim 3$ coronal outflow due to convective instabilities and magnetic buoyancy (McKinney & Gammie 2004). This component is sufficiently relativistic to explain the jets from black hole (and most neutron star) x-ray binary systems. This mechanism only requires a thick disk and not necessarily a spinning black hole, where other unification models suggest that the black hole spin is necessary (Meier 2001).

It has been suggested that the transient, more relativistic, jet produced in GRS 1915+105 is the result the formation of a thin disk as the ADAF collapses as the mass accretion rate increases (Fender et al. 2004b). No particular model of the transient jet has been suggested.

Here we give a proposal for the disk-jet coupling in black hole x-ray binary systems, such as GRS 1915+105. In the prolonged hard x-ray state the disk is ADAF-like and the system produces a Poynting synchrotron self-absorbed jet with $\Gamma \lesssim 2$, which may be partially or completely Compton dragged to nonrelativistic speeds. However, in the thick state, a Poynting-baryon jet is produced with $\Gamma \sim 1.5$. During the soft state, the disk is SS-like (Shakura & Sunyaev 1973) and the black hole polar field is relatively weak and the system generates an uncollimated (more radial) weak optically thin Poynting outflow. During this phase there is also a weak non-relativistic uncollimated Poynting-baryon outflow.

During the transition between hard and soft x-ray states the production of pairs decreases significantly in the funnel, but the black hole polar magnetic field has yet to decay. During this transition, an optically thin Poynting-lepton jet with $\Gamma \sim 2-3$ is produced that is collimated by the remaining inner-radial ADAF-like structure or the Poynting-baryon wind that was produced prior. The Lorentz factor produced in the transition depends on the details of the disk structure, and so γ-ray emission, during the transition. Once the black hole field has decayed, the fast transient jet shuts down.

Alternatively, during the transition to the high-soft state a transient jet can emerge as the corona is suddenly exposed to more Poynting flux from the black hole. This last bit of coronal material can be launched off as a faster transient baryon-loaded jet. The dynamics of the state transition is left for future work. This overall picture is in basic agreement with Fender & Belloni (2004), with the additional physics of pair creation dominating the Poynting-lepton jet formation process.

It is interesting that the results of Gierliński & Done (2004) suggest that for at least some black hole x-ray binaries that have jets, the black hole is likely not rapidly rotating (i.e. perhaps $j \lesssim 0.5$). For such black holes, there is negligible Poynting flux in the form of a Poynting-dominated jet (McKinney & Gammie 2004). Thus, our conclusion that black hole x-ray binary jets are driven by coronal outflows is consistent with the results of Gierliński & Done (2004). However, even if black hole x-ray binaries were rapidly rotating they might not produce Poynting-dominated jets.

SS443 is plausibly an $M \sim 20\mathrm{M}_\odot$ black hole system that has a jet with $v \sim 0.3c$ (Lopez et al. 2003). Such a low jet velocity can be explained by a Poynting-baryon jet. To explain the opening angle of $\sim 1^\circ$ the disk should be very thick near the black hole, while the pulsed jet features can be explained as an instability due to the overly thick disk self-interacting at the poles near the black hole.

6. SUMMARY OF COMPANION PAPER NUMERICAL RESULTS

This section summarizes the results of McKinney (2005b) using a GRMHD code HARM (Gammie et al. 2003a) with an advanced inversion method (Noble et al. 2005). Kerr-Schild coordinates were used in order to avoid numerical artifacts associated with causal interactions between the inner-radial boundary and the rest of the flow. Viscous models have found this issue to be critical to avoid spurious fluctuations in the jet (McKinney & Gammie 2002), such as might be associated with codes using Boyer-Lindquist coordinates.

6.1. *Jet propagation*

As described in detail in McKinney (2005b) and as shown in figure 3 and 4, the Poynting-dominated jet forms as the differential rotation of the disk and the frame-dragging of the black hole induce a significant toroidal field that launches material away from the black hole by the same force described in equation C14.

A coronal outflow is also generated between the disk and Poynting-dominated jet. In this model the coronal outflow has $\Gamma_\infty \sim 1.5$. The coronal-funnel boundary contains shocks with a sonic Mach number of $M_s \sim 100$. The inner-radial interface between the disk and corona is a site of vigorous reconnection due to the magnetic buoyancy and convective instabilities present there. These two parts of the corona are about 100 times hotter than the bulk of the disk. Thus these coronal components are a likely sites for Comptonization and nonthermal particle acceleration.

Figure 3 and figure 4 show the final log of density and magnetic field projected on the Cartesian z vs. x plane. For the purposes of properly visualizing the accretion flow and jet, we follow MacFadyen & Woosley (1999) and show both the negative and positive x-region by duplicating the axisymmetric result across the vertical axis. Color represents $\log(\rho_0/\rho_{0,disk})$ with dark red highest and dark blue lowest. The final state has a density maximum of $\rho_0 \approx 2\rho_{0,disk}$ and a minimum of $\rho_0 \sim 10^{-13}\rho_{0,disk}$ at large radii. Grid zones are not smoothed to show grid structure. Outer radial zones are large, but outer θ zones are below the resolution of the figure.

Clearly the jet has pummelled its way through the surrounding medium, which corresponds to the stellar envelope in the collapsar model. By the end of the simulation, the field has been self-consistently launched in to the funnel region and has a regular geometry there. In the disk and at the surface of the

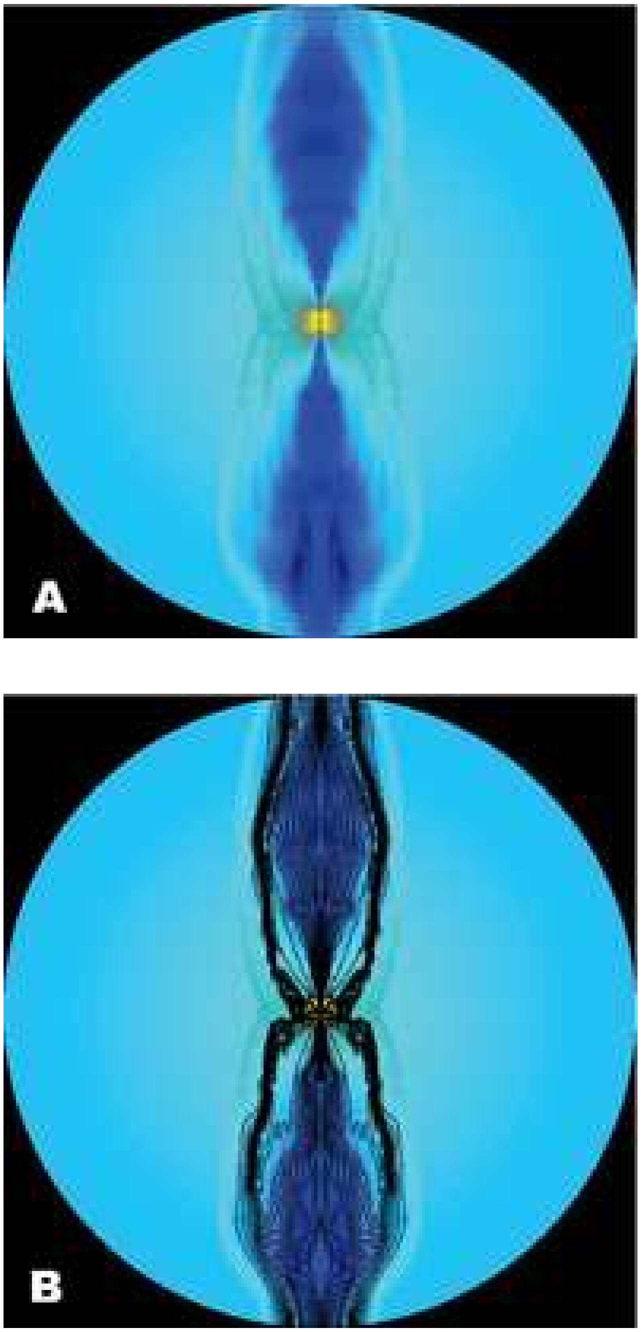

FIG. 3.— Jet has pummelled its way through presupernova core and through $1/10$th of entire star. Panel (A) shows final distribution of $\log\rho_0$ on the Cartesian plane. Black hole is located at center. Red is highest density and black is lowest. Panel (B) shows magnetic field overlayed on top of log of density. Outer scale is $r = 10^4 GM/c^2$.

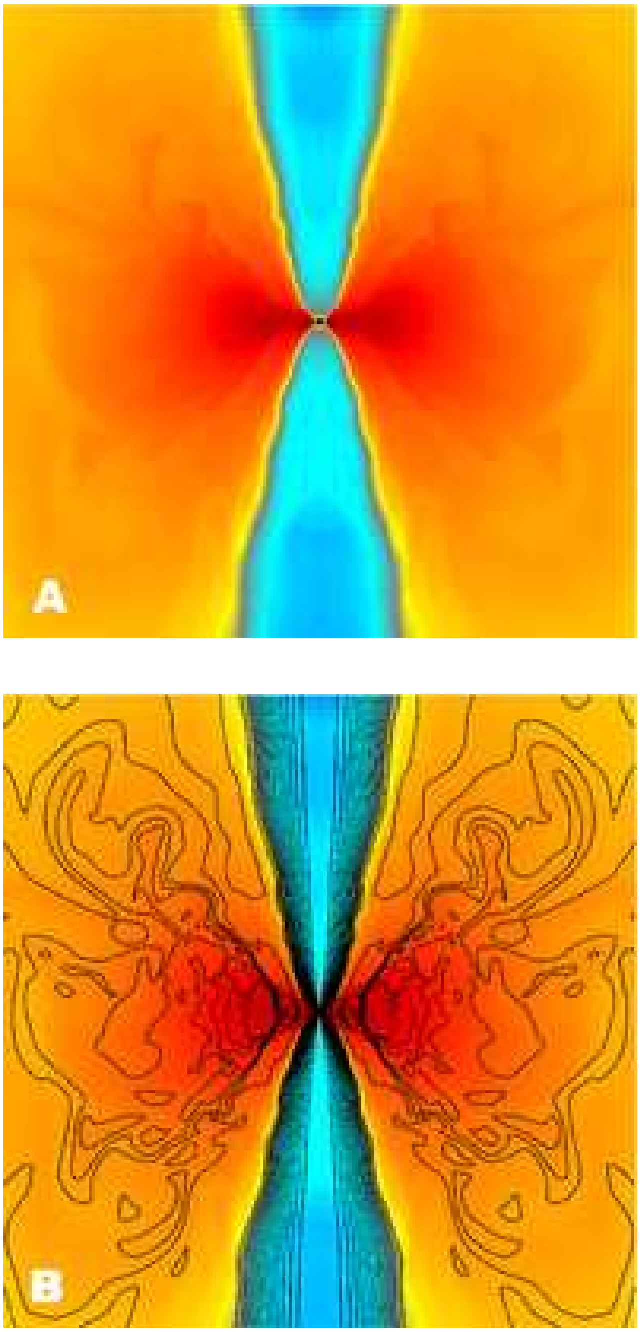

FIG. 4.— Strongest magnetic field near black hole in X-configuration due to Blandford-Znajek effect and collimation of disk+coronal outflow. As in figure 3, but outer scale is $r = 10^2 GM/c^2$. Black hole is black circle at center. Color scale is same as in figure 3.

disk the field is curved on the scale of the disk scale height. Within $r \lesssim 10^2 r_g$ the funnel field is ordered and stable due to the poloidal field dominance. However, beyond $r \sim 10^2 r_g$ the poloidal field is relatively weak compared to the toroidal field and the field lines bend and oscillate erratically due to pinch instabilities. The radial scale of the oscillations is $10^2 r_g$ (but up to $10^3 r_g$ and as small as $10 r_g$), where $r \sim 10 r_g$ is the radius where poloidal and toroidal field strengths are equal. By the end of the simulation, the jet has only fully evolved to a state independent of the initial conditions at $r \approx 5 \times 10^3 r_g$, beyond which the jet features are a result of the tail-end of the initial launch of the field. The head of the jet has passed beyond the outer boundary of $r = 10^4 r_g$. Notice that the magnetic field near the black hole is in an X-configuration. This is due to the BZ-effect having power $P_{jet} \propto \sin^2\theta$, which vanishes at the polar axis. The X-configuration is also related to the fact that the disk+corona is collimating the Poynting-dominated jet. The field is mostly monopolar near the black hole, and such field geometries *decollimate* for rapidly rotating black holes in force-free electrodynamics (Krasnopolsky et al. 2005).

6.2. *Summary of Fits*

A summary of the fits along a fiducial field line is given. Near the black hole the half-opening angle of the full Poynting-dominated jet is $\theta_j \sim 1.0$, while by $r \sim 120r_g$, $\theta_j \sim 0.1$. This can be roughly fit by

$$\theta_j \sim \left(\frac{r}{r_g}\right)^{-0.4} \quad \text{(inner)} \tag{63}$$

for $r < 120r_g$ and $\theta_j \sim 0.14$ beyond. The core of the jet follows a slightly stronger collimation with

$$\theta_j \propto r^{-2/5} \tag{64}$$

up to $r < 120r_g$ and $\theta_j \sim 0.09$ beyond. Also, roughly for M87 and the collapsar model, the core of the jet has

$$\Gamma_{bulk} \sim \left(\frac{r}{5r_g}\right)^{0.44} \quad \text{(inner)} \tag{65}$$

for $5 < r \lesssim 10^3 r_g$ and constant beyond for the M87 model if including synchrotron radiation, while the collapsar model should continue accelerating and the power law will truncate when most of the internal and Poynting energy is lost to kinetic energy and the jet becomes optically thin at about $r \sim 10^9 r_g$ or internal shocks take the energy away. If the acceleration is purely thermal without any magnetic effect, then $\Gamma \propto r$ (Mészáros & Rees 1997). However, it is not clear how the equipartition magnetic field affects the acceleration. Roughly for GRS 1915+105 the core of the jet has

$$\Gamma_{bulk} \sim \left(\frac{r}{5r_g}\right)^{0.14} \quad \text{(inner)} \tag{66}$$

for $5 < r \sim 10^3 r_g$ and constant beyond, with no account for Compton drag or pair annihilation. Also, for any jet system the base of the jet has $\rho_0 \propto r^{-0.9}$ (inner) for $r \lesssim 120r_g$ and $\rho_0 \propto r^{-2.2}$ (outer) beyond. For the collapsar and M87 models

$$\frac{\rho_0}{\rho_{0,disk}} \sim 1.5\times10^{-9}\left(\frac{r}{120r_g}\right)^{-0.9} \quad \text{(inner)} \tag{67}$$

and

$$\frac{\rho_0}{\rho_{0,disk}} \sim 1.5\times10^{-9}\left(\frac{r}{120r_g}\right)^{-2.2} \quad \text{(outer)}, \tag{68}$$

while for GRS 1915+105 the inner-radial coefficient is 10^{-5} and outer is 6×10^{-3}. For the collapsar model, the inner radial internal energy density is moderately fit by

$$\frac{u}{\rho_{0,disk}c^2} = 4.5\times10^{-9}\left(\frac{r}{120r_g}\right)^{-1.8} \quad \text{(inner).} \tag{69}$$

The outer radial internal energy density is moderately fit by

$$\frac{u}{\rho_{0,disk}c^2} = 4.5\times10^{-9}\left(\frac{r}{120r_g}\right)^{-1.3} \quad \text{(outer).} \tag{70}$$

The transition radius is $r \approx 120r_g$. For M87 the internal energy is near the rest-mass density times c^2 until $r \sim 120r_g$ when the dependence is as for the collapsar case. For GRS1915+105 the internal energy is near the rest-mass density times c^2 until $r \sim 120r_g$ and then rises to about 2.5 times the rest-mass density times c^2. The inner radial toroidal lab field is well fit by

$$\frac{B^{\hat\phi}}{\sqrt{\rho_{0,disk}c^2}}[\text{Gauss}] = 0.0023\left(\frac{r}{390r_g}\right)^{-0.7} \quad \text{(inner)} \tag{71}$$

for $5 < r < 390r_g$. The outer radial toroidal lab field is well fit by

$$\frac{B^{\hat\phi}}{\sqrt{\rho_{0,disk}c^2}}[\text{Gauss}] = 0.0023\left(\frac{r}{390r_g}\right)^{-1.5} \quad \text{(outer)} \tag{72}$$

for $r > 390r_g$.

For the typical jet with no atypical pinch instabilities, the energy and velocity structure of the jet follow

$$\epsilon(\theta) = \epsilon_0 e^{-\theta^2/2\theta_0^2}, \tag{73}$$

where $\epsilon_0 \approx 0.18$ and $\theta_0 \approx 8^\circ$. The total luminosity per pole is $L_j \approx 0.023\dot{M}_0 c^2$, where 10% of that is in the “core” peak Lorentz factor region of the jet within a half-opening angle of 5°. Also, Γ_∞ is approximately Gaussian

$$\Gamma_\infty(\theta) = \Gamma_{\infty,0} e^{-\theta^2/2\theta_0^2}, \tag{74}$$

where $\Gamma_{\infty,0} \approx 3\times10^3$ and $\theta_0 \approx 4.3^\circ$. Also, Γ is approximately Gaussian

$$\Gamma(\theta) = \Gamma_0 e^{-\theta^2/2\theta_0^2}, \tag{75}$$

where $\Gamma_0 \approx 5$ and $\theta_0 \approx 11^\circ$. The outer sheath’s ($\theta \approx 0.2$) seed photon temperature as a function of radius is

$$T_{\gamma,seed} \sim 50\text{keV}\left(\frac{r}{5\times10^3 r_g}\right)^{-1/3}. \tag{76}$$

7. DISCUSSION

For GRB jets, the injected Poynting flux probably dominates the injected energy flux provided by neutrino annihilation. This poses problems for the classic neutrino-driven fireball model. Super-efficient neutrino emission mechanisms with an *average* neutrino energy of 210MeV are required in order for the neutrino annihilation energy to be as large as the energy provided by the BZ effect. However, the BZ effect itself might operate in a super-efficient mode once flux has accumulated near the black hole (Narayan et al. 2003). This vertical field threading the disk leads up to 5 times larger luminosity (McKinney & Gammie 2004), in which case an average neutrino energy of 1000MeV is required to compete with the BZ-effect.

For GRBs, equation 42 shows that slightly less rapidly rotating black holes would generate slightly less Lorentz factors but achieve a lower luminosity. This is consistent with the observation that harder long-duration bursts have higher luminosity, and so suggests that small changes in the stellar rotation rate might determine the hardness of long-duration bursts.

The fact that blazars are less luminous for increasing hardness could be explained by the dependence on the jet Lorentz factor on the pair creation physics. Blazars could have similar black hole spin, but the hardness of their emission is determined by the jet Lorentz factor. Lower luminosity systems load the jet with less pairs and so the Lorentz factor is larger. Compton drag of environment or disk reflected seed photons can then upscatter to very large energy, such as observed in TeV-emitting BL-Lac objects.

Our results suggest that radiatively efficient x-ray binaries, such as GRS1915+105, may only exhibit a relativistic Poynting-baryon jet. In particular, such a jet is relativistic only in the low-hard state when the disk is geometrically thick.

8. CONCLUSIONS

Primarily two types of relativistic jets form in black hole (and perhaps neutron star) systems. The Poynting-dominated jet region is composed of field lines that connect the rotating black hole to large distances. Since the ideal MHD approximation holds very well, the only matter that can cross the field lines are neutral particles, such as neutrinos, photons, and free neutrons.

The primary differences between GRBs, AGN, and black hole x-ray binaries is the pair-loading of the Poynting-dominated jet, a similar mass-loading by free neutrons in GRB-type systems, the optical depth of the jet, and the synchrotron cooling timescale of the jet.

For GRB-type systems the neutron diffusion flux is sufficiently large to be dynamically important, but small enough to allow $\Gamma \sim 100-1000$. Beyond $r \sim 10 r_g$ many of the electron-positron pairs annihilate, so the Poynting-dominated jet is dominated in mass by electron-proton pairs from collision-induced neutron decay. Most of the energy is provided by the BZ effect instead of neutrino-annihilation.

For AGN and x-ray binaries, the density of electron-positron pairs established near the black hole primarily determines the Lorentz factor at large distances. Radiatively inefficient AGN, such as M87, achieve $2 \lesssim \Gamma_\infty \lesssim 10$ and are synchrotron cooling limited. The lower the γ-ray radiative efficiency of the disk, the more energy per particle is available in the shock-zone. Radiatively efficient systems such as GRS1915+105 likely have no Poynting-lepton jet due to strong pair-loading and destruction by Comptonization by the plentiful soft photons for x-ray binaries with optically thick jets. However, all these systems have a mildly relativistic, baryon-loaded jet when in the hard-low state when the disk is geometrically thick, which can explain jets in most x-ray binary systems.

In an companion paper McKinney (2005b), a GRMHD code, HARM, with pair creation physics was used to evolve many black hole accretion disk models. The basic theoretical predictions made in this paper that determine the Lorentz factor of the jet were numerically confirmed. However, Poynting flux is not necessarily directly converted into kinetic energy, but rather Poynting flux is first converted into enthalpy flux into a “magnetic fireball” due to shock heating. Thus, at large distances the acceleration is primarily thermal, but most of that thermal energy is provided by shock-conversion of magnetic energy. In GRB systems this magnetic fireball leads to thermal acceleration over an extended radial range. The jets in AGN and x-ray binaries release this energy as synchrotron and inverse Compton emission and so the jet undergoes negligible thermal acceleration beyond $r \sim 10^2 - 10^3 r_g$.

Based upon prior numerical (McKinney 2005b) and this theoretical work, basic conclusions for collapsars include:

1. Black hole energy, not neutrino energy, typically powers GRBs.
2. Poynting-dominated jets are mostly loaded by $e^- e^+$ pairs close to the black hole, and by $e^- p$ pairs for $r \gtrsim 10 r_g$.
3. BZ-power and neutron diffusion primarily determines Lorentz factor.
4. Variability is due to toroidal field instabilities.
5. Poynting flux is converted into enthalpy flux and leads to the formation of a “magnetic fireball.”
6. Patchy jet develops $10^2 \lesssim \Gamma_\infty \lesssim 10^3$, as required by internal shock model.
7. Random number of patches (< 1000 for 30 second burst) and so random number of pulses.
8. Energy structure of jet is Gaussian with $\theta_0 \approx 8°$.
9. Core of jet with $\theta_j \approx 5°$ can explain GRBs.
10. Extended slower jet component with $\theta_j \approx 25°$ can explain x-ray flashes.
11. Coronal outflows with $\Gamma \sim 1.5$ may power supernovae (by producing, e.g., ^{56}Ni) with $M \sim 0.1 M_\odot$ processed by corona.

Based upon prior numerical (McKinney 2005b) and this theoretical work, basic conclusions for AGN or x-ray binaries include:

1. Poynting-dominated jets $e^- e^+$ pair-loaded unless advect complicated field.
2. γ-ray radiative efficiency, and so pair-loading, determines maximum possible Lorentz factor.
3. Poynting-lepton jet is collimated with $\theta_j \approx 5°$.
4. Extended slow jet component with $\theta_j \lesssim 25°$.
5. For fixed accretion rate, variability is due to toroidal field instabilities.
6. Poynting flux is shock-converted into enthalpy flux.
7. In some AGN, shock heat in transonic transition lost to synchrotron emission and limits achievable Lorentz factor to $2 \lesssim \Gamma \lesssim 10$ (e.g. in M87).
8. Coronal outflows produce broad inner-radial jet features in AGN together with well-collimated jet component (e.g. in M87).
9. In some x-ray binaries, Compton drag loads Poynting-lepton jets and limits Poynting-lepton jet to $\Gamma \lesssim 2$ or jet destroyed.
10. In some x-ray binaries, Poynting-lepton jet optically thick and emits self-absorbed synchrotron.
11. Coronal outflows have collimated edge with $\Gamma \lesssim 1.5$.
12. Coronal outflows may explain all mildly relativistic and nonrelativistic jets in radiatively efficient systems (most x-ray binaries).

For AGN and X-ray binaries, the coronal outflow collimation angle is strongly determined by the disk thickness. The above assumed $H/R \sim 0.2$ near the black hole and $H/R \sim 0.6$ far from the black hole, while $H/R \sim 0.9$ (ADAF-like) is perhaps more appropriate for some systems. The sensitivity of these results to H/R is left for future work.

ACKNOWLEDGMENTS

I thank Avery Broderick for an uncountable number of inspiring conversations. I also thank Charles Gammie, Brian Punsly, Amir Levinson, and Ramesh Narayan, with whom each I have had inspiring conversations. This research was supported by NASA-ATP grant NAG-10780 and an ITC fellowship.

APPENDIX

A. PAIR CREATION NOTES

The electron-positron pair plasma that forms may annihilate itself into a fireball if the pair annihilation rate is faster than the typical rate of the jet (c^3/GM) near the black hole. Also, if the pair annihilation timescale is shorter than the dynamical time, then pair annihilation would give a collisional term in the Boltzmann equation. From the pair annihilation rate given by equation D7, one finds that $t_{pa} \gg GM/c^3$ for AGN and marginally so for x-ray binaries. Thus, pairs mostly do not annihilate, and so formally the pair plasma that forms in the low-density funnel region is collisionless so that the Boltzmann equation should be solved directly. Plasma instabilities and relativistic collisionless shocks are implicitly assumed to keep the pairs in thermal equilibrium so the fluid approximation remains mostly valid, as is a good approximation for the solar wind (see, e.g. Feldman & Marsch 1997; Usmanov et al. 2000). This same approximation has to be invoked for the thick disk state in AGN and x-ray binaries, such as for the ADAF model (McKinney 2004). For regions that pair produce slower than the jet dynamical time, each pair-filled fluid element has a temperature distribution that gives an equation of state with $P = \rho_{0,e^-e^+} k_b T_e/m_e$ rather than $P = (11/12)aT^4$, where a is the radiation constant. So most of the particles have a Lorentz factor of $\Gamma_e \sim u/(\rho_{0,e^-e^+}c^2)$ and little of the internal energy injected is put into radiation. This also allow the use of a single-component approximation. A self-consistent Boltzmann transport solution is left for future work.

On the contrary for GRB systems, due to the relatively high density of pairs, the time scale for pair annihilation is $t_{pa} \ll GM/c^3$ along the entire length of the jet. Thus a pair fireball forms and the appropriate equation of state is that of an electron-positron-radiation fireball. Thus, formally the pair fireball rest-mass density is not independent of the pair fireball internal energy density. However, because the pairs are well-coupled to the radiation until a much larger radius of $r \sim 10^8 - 10^{10} r_L$, the radiation provides an inertial drag on the remaining pair plasma. That is, the relativistic fluid energy-momentum equation is still accurate. So the effective rest-mass density is $\sim \rho_0 + u$ (u the total internal energy of the fireball), and so the effective rest-mass is independent of the cooling of the fireball until the fireball is optically thin (see, e.g., Mészáros & Rees 1997).

For GRB systems, the mass conservation equation is reasonably accurate. Even though the electron-positron pairs annihilate, the rest-mass of pairs injected is approximately that of the pairs that are injected due to Fick-diffusion of neutrons (see next section). The annihilation energy from electron-positron pairs contributes a negligible additional amount of internal energy, so can be neglected, especially compared to the Poynting energy flux that emerges from the black hole. Thus, the rest-mass can always be assumed to be due to baryons rather than the electron-positron pairs. This also suggests that the neutrino annihilation is a negligible effect if the BZ power is larger than the neutrino annihilation power.

In summary, the rest-mass evolution discussed in McKinney (2005b) are accurate for GRB, AGN, and marginally so for x-ray binaries. This is despite the lack of Boltzmann transport for the collisional system, or a collisional term due to pair annihilation.

A.1. *Baryon Contamination*

Notice that some fraction of baryons contaminate the jet due to neutron diffusion and subsequent collisional cascade into an electron-proton plasma (Levinson & Eichler 2003). They estimate the diffusion using Fick's law. First, the role of ambipolar diffusion is considered (see, e.g. Shu 1992, chpt. 27). The drift velocity is

$$v_{drift,pn} \sim \frac{B^2}{4\pi\gamma_{pn} n_p m_p n_n m_n L}, \tag{A1}$$

where $L \sim r(H/R)$ is the typical field radius of curvature induced by disk turbulence and

$$\gamma_{pn} = \frac{\langle \sigma_{pn} v_{rel,pn} \rangle}{m_p + \rho/m_n} \tag{A2}$$

is the drag coefficient and $\langle \sigma v \rangle \sim 40c \times 10^{-27}$. The drift velocity can also be written as

$$v_{drift,pn}/c \sim \left(\frac{b^2}{\rho c^2}\right)\left(\frac{m_n c}{\langle \sigma v \rangle \rho r(H/R)}\right). \tag{A3}$$

Assuming all the diffused neutrons are converted to protons+electrons and carried with the outflow, then the diffusion flux is

$$F = \rho v_{drift,pn} = \frac{b^2}{\rho c^2}\frac{m_n c^2}{\langle \sigma v \rangle r(H/R)}. \tag{A4}$$

and the mass flux across an axisymmetric conical outflow is

$$\dot{M}_{inj,ambi} = 2\pi \int_0^{r_{out}} Fr dr \tag{A5}$$

and so

$$\dot{M}_{inj,ambi} = 2\pi (Fr) r_{out} \tag{A6}$$

GRB numerical GRMHD models show that the coronal region next to the Poynting-dominated jet has a time-averaged value of $b^2/(\rho c^2) \sim 1$ and the turbulent induced eddies occur when the disk has $H/R \sim 0.2$ (McKinney & Gammie 2004; McKinney 2004). This gives a mass flux vs. radius of

$$\dot{M}_{inj,ambi} \sim 10^{-14}\left(\frac{r - r_{stag}}{r_g}\right)\dot{M}_{acc}, \tag{A7}$$

where pairs that enter inside $r \lesssim r_{stag}$ fall into the black hole and do not load the jet. For a recombination radius of $r_n \sim 2\times10^9$cm (Levinson & Eichler 2003), this gives

$$\dot{M}_{inj,ambi} \sim 4\times10^{-10}\dot{M}_{acc}. \tag{A8}$$

This can be compared to the result of Levinson & Eichler (2003) for Fick-diffusion, where the mass injection rate of free-streaming particles (their eq. 7) is

$$\dot{M}_{inj,Fick} \sim 3\times10^{-7}\left(\frac{r}{r_g}\right)^{2/3}\dot{M}_{acc} \tag{A9}$$

for their collapsar model with jet half-opening angle of $\theta_j = 0.1$, specific enthalpy $h \sim 1$, $L_j \sim 10^{51}\,\mathrm{erg\,s^{-1}}$, a neutron thermal velocity of $v \sim 0.1c$. The thermal velocity is based upon the near-funnel coronal value of $u/(\rho_0 c^2) \sim 0.01-0.1$ as measured from GRMHD numerical models. Notice that this ratio is typically 0.01 in the corona, but is 0.1 at the edge, so we use 0.1 since the Fick diffusion is based upon the edge values. Notice that they used $v \sim c$. For a recombination radius of $r_n \sim 2\times10^9$cm after which no more free neutrons exist, one has that

$$\dot{M}_{inj,Fick} \sim 7\times10^{-5}\dot{M}_{acc}. \tag{A10}$$

Hence, Fick diffusion dominates ambipolar diffusion. The role of reconnection, between the corona/coronal wind and jet, in loading the jet with baryons is left for future work.

The characteristic timescale for moving these pairs is $\sim t_g(r/r_g)$ and characteristic length is $\sim r_g(r/r_g)$, so a characteristic density vs. radius is

$$\rho_{pe^-} \sim \frac{\dot{M}_{inj,Fick}t_g}{r_g^3}\left(\frac{r}{r_g}\right)^{-2} \sim 3\times10^{-7}\left(\frac{r}{r_g}\right)^{-4/3}\rho_{0,disk}. \tag{A11}$$

Notice that this is comparable to the rest-mass in pairs given by equation 18. Thus, as the fireball decays in pair rest-mass, the rest-mass quickly becomes dominated by neutrons diffusing across the magnetic wall between the corona and funnel. Hence, the baryon conservation law holds and the approximations used here hold well. A pair-annihilation term is only needed to account for the contribution to the internal energy. Since $f_\rho \sim 8f_h$, this contribution is a $\sim 10\%$ effect and is not expected to affect the results of the numerical models of McKinney (2005b).

A.2. *Pair-Radiation Equation of State*

The total amount of comoving energy put into the thermal fireball is

$$\begin{aligned} u_{0,tot} &= \rho_{0,e^-e^+}c^2 + u_{0,e^-e^+} + u_{0,\gamma} = \\ &AT^4\int_0^\infty dx\frac{x^2\sqrt{x^2+\tilde{m}^2}}{e^{\sqrt{x^2+\tilde{m}^2}}+1} + u_{0,\gamma}, \end{aligned} \tag{A12}$$

where $u_{0,\gamma} = 1.62348AT^4$, $A = 4.66244\times10^{-15}\,\mathrm{erg\,cm^{-3}K^{-4}}$, $x \equiv pc/k_bT$, $\tilde{m} \equiv m_ec^2/k_bT$, p is the momentum in the fluid frame, and the rest-number density of photons is $n_\gamma = 20.2944\,\mathrm{cm^{-3}}T^3$. The rest-mass in pairs is

$$\rho_{0,e^-e^+} = BT^3\int_0^\infty dx\frac{x^2}{e^{\sqrt{x^2+\tilde{m}^2}}+1}, \tag{A13}$$

where $B = 3.07589\times10^{-26}\,\mathrm{g\,cm^{-3}K^{-3}}$, and the number density of pairs is $n_{0,e^-e^+} = \rho_{0,e^-e^+}/m_e$. Notice that the GRMHD equations of motion relate the comoving energy to energy at infinity by

$$u_{tot} = u_{0,tot}u^tu_t + p_{gas} = (f_\rho + f_h + f_m)e_{\nu\bar{\nu},ann} \tag{A14}$$

and $\rho_{e^-e^+} = \rho_{0,e^-e^+}u^t$, where

$$p_{gas} = \frac{AT^4}{3}\int_0^\infty dx\frac{x^2\sqrt{x^2+\tilde{m}^2}}{e^{\sqrt{x^2+\tilde{m}^2}}+1} + p_{0,\gamma}, \tag{A15}$$

and $p_\gamma = u_{0,\gamma}/3$. This gives sufficient information to solve for u^t and u_t or $\dot{\rho}_{e^-e^+} = \partial/\partial t(\rho_{0,e^-e^+}u^t)$. The study of McKinney (2005b) uses a fixed γ-law gas equation of state with $\gamma = 4/3$ to model the typically radiation-dominated system.

B. IDEAL MHD QUANTITIES CONSERVED ALONG EACH FLOW LINE

Kerr spacetime is stationary and axisymmetric with 2 Killing vectors $\xi^\mu_t = \frac{\partial}{\partial_t} = -\delta^\mu_t$ and $\xi^\phi_\mu = \frac{\partial}{\partial\phi} = \delta^\mu_\phi$ that satisfy $\mathcal{L}_\xi(\mathbf{g}) = 0$, where $\mathcal{L}$ is the Lie derivative and $\mathbf{g}$ is the metric. For a vector X^μ, tensors $\mathbf{T}$ that obey $\mathcal{L}_X(\mathbf{T}) = 0$ are conserved along X. In particular, for $X = \xi$, such a tensor is a physical quantity independent of the ignorable coordinates t and ϕ. For $X = u$, the 4-velocity, the tensor is conserved along each flow line. One can derive a set of conserved flow quantities that are associated with the Killing symmetries (Bekenstein & Oron 1978). The below summarizes those results that are key to this paper. This presentation is necessary for the discussion regarding the determination of the Lorentz factor of the jet.

In the ideal MHD approximation one can show that $\mathcal{L}_u(\xi^\mu A_\mu) = 0$, where $F_{\mu\nu} \equiv A_{\nu,\mu} - A_{\mu,\nu}$ defines the vector potential A_μ. Thus for an unsteady axisymmetric flow the ϕ component of the magnetic vector potential ($A_\phi = \xi^\mu_\phi A_\mu$) is conserved along each flow line, while for a steady non-axisymmetric flow the electric potential ($A_t = \xi^\mu_t A_\mu$) is conserved along each flow line.

Bekenstein & Oron (1978) also show that there are four other independent conserved scalar quantities for an axisymmetric, stationary fluid. These correspond to the first integrals of Maxwell's equation ${}^{*}F^{\mu\nu}_{;\mu} = 0$ and the conservation equation $T^{\mu}_{\nu;\mu} = 0$ with the use of the continuity equation $(\rho_0 u^{\mu})_{;\mu} = 0$. These first integrals are associated with the projection of the 2 Killing vectors and the magnetic field (b^{μ}) on these equations of motion.

For a degenerate (${}^{*}F^{\mu\nu}F_{\mu\nu} = e^{\mu}b_{\mu} = 0$), stationary and axisymmetric plasma, one finds

$$A_{\phi,\theta}A_{t,r} - A_{t,\theta}A_{\phi,r} = 0. \tag{B1}$$

It follows that one may write

$$\frac{A_{t,\theta}}{A_{\phi,\theta}} = \frac{A_{t,r}}{A_{\phi,r}} \equiv -\Omega_F(r,\theta) \tag{B2}$$

where Ω_F is usually interpreted as the "rotation frequency" of the electromagnetic field (this is Ferraro's law of isorotation; see e.g. Frank, King, & Raine 2002, §9.7 in a nonrelativistic context). Notice that $\Omega_F \equiv F_{tr}/F_{r\phi} = F_{t\theta}/F_{\theta\phi}$. One can show in the ideal MHD approximation that

$$\Omega_F = v^{\phi} - B^{\phi}v^{\theta}/B^{\theta} = v^{\phi} - B^{\phi}v^{r}/B^{r} \tag{B3}$$

is conserved along each flow line. The first term corresponds to fluid rotation and the second term corresponds to the slip along the toroidal component of a field line. This yields $F_{\mu\nu}$ in terms of the free functions Ω_F, A_{ϕ}, and B^{ϕ}. Thus, $F_{rt} \equiv \sqrt{-g}E_r = -\Omega_F A_{\phi,r}$, $F_{\theta t} \equiv \sqrt{-g}E_{\theta} = -\Omega_F A_{\phi,\theta}$, $F_{r\theta} = \sqrt{-g}B^{\phi}$, $F_{\phi r} = \sqrt{-g}B^{\theta} = -A_{\phi,r}$, and $F_{\theta\phi} = \sqrt{-g}B^{r} = A_{\phi,\theta}$. The diagonal components are zero and $F_{\phi t} \equiv E_{\phi} = 0$, where $B^{i} \equiv {}^{*}F^{it}$, $E_i \equiv F_{it}/\sqrt{-g}$ such that $B^{i}E_i = {}^{*}F^{\mu\nu}F_{\mu\nu}/(4\sqrt{-g}) \equiv E\cdot B$. Thus for fixed poloidal magnetic field, Ω_F is a measure of the electric field. With the Faraday written in terms of B^{i} and Ω_F, the electromagnetic field automatically satisfies the source-free Maxwell equations.

Using similar constraints on $F^{\mu\nu} = A^{\nu,\mu} - A^{\mu,\nu}$ and with $E^{i} \equiv F^{it}\sqrt{-g}$, $B_i \equiv {}^{*}F_{it}$, one can show that $\sqrt{-g}F^{rt} \equiv E^{r} = \tau_{\theta}B_{\theta}$, $\sqrt{-g}F^{\theta t} \equiv E^{\theta} = -\tau_r B_r$, $\sqrt{-g}F^{\phi t} \equiv E^{\phi} = \tau_{\phi}B_{\phi}$, $\sqrt{-g}F^{r\theta} = -B_{\phi}$, and $\sqrt{-g}F^{r\phi} = B_{\theta}$, $\sqrt{-g}F^{\theta\phi} = -B_r$. Here there is only one independent quantity among the three τ_i's that are set by ${}^{*}F_{\mu\nu}F^{\mu\nu} = 0$ and that the flow and metric are stationary and axisymmetric (i.e. $E_{\phi} = 0$). One can show that $\tau_{\phi} = B_r B_{\theta}(\tau_r - \tau_{\theta})/B_{\phi}^2$ and solve for another by using $E_{\phi} = F^{\alpha\beta}g_{\alpha t}g_{\beta\phi} = 0$.

It is interesting to note that in Boyer-Lindquist coordinates $\tau_{\phi} = 0$ and $\tau_r = \tau_{\theta} \rightarrow \tau$ and then the contravariant and covariant Faraday take on the same simple form with

$$\tau = -\frac{g^{t\phi} - g^{tt}\Omega_F}{g^{\phi\phi} - g^{t\phi}\Omega_F} = \frac{\Omega_F/\Omega_{ZAMO} - 1}{\Omega_0 - \Omega_F}, \tag{B4}$$

where $\Omega_{ZAMO} \equiv g^{t\phi}/g^{tt} = 2ar/A$ is the angular frequency of a zero angular momentum observer (ZAMO) and

$$\Omega_0 \equiv g^{\phi\phi}/g^{t\phi} = \frac{a^2 - \Delta/\sin^2\theta}{2ar}. \tag{B5}$$

Notice that if $\Omega_F = \Omega_{ZAMO}$, then $\tau = 0$ and so $E^{i} = 0$. So the difference between the dragging of inertial frames and the field rotation frequency generates the electric field E^{i}. Also in Boyer-Lindquist $B_r = B^{r}|g|g^{\theta\theta}g^{\phi\phi}(\Omega_F/\Omega_0 - 1)$, where $|g|g^{\theta\theta}g^{\phi\phi} = (\Sigma - 2r)/\Delta$. Also, $B_{\theta} = B^{\theta}|g|g^{rr}g^{\phi\phi}(\Omega_F/\Omega_0 - 1)$, where $|g|g^{rr}g^{\phi\phi} = \Sigma - 2r$. Also, $B_{\phi} = -B^{\phi}|g|g^{rr}g^{\theta\theta}$, where $|g| \equiv |\mathrm{Det}(g_{\mu\nu})|$ and $|g|g^{rr}g^{\theta\theta} = \Delta\sin^2\theta$.

Using the definition of $F^{\mu\nu}$ given above one can define A_{ϕ} in terms of the poloidal B^{r} and B^{θ} giving

$$A_{\phi}(l_f) - A_{\phi}(l_i) = \int_{l_i}^{l_f}(\sqrt{-g}(B^{r}d\theta - B^{\theta}dr)) \tag{B6}$$

over the line segment from l_i to l_f. Thus given the poloidal field components, then A_{ϕ} can be determined up to a constant. The contours of constant A_{ϕ} represent time-dependent poloidal magnetic field surfaces for any ϕ. Shown in Cartesian coordinates, beyond a few gravitational radii from even a $j = 1$ black hole, the density of lines represents the field strength in the lab frame. Near the horizon where the intrinsic volume of space is larger than in Minkowski space-time, the density of field lines in such a Cartesian plot overestimates the lab frame field strength by factors of $\lesssim 2$.

For an inviscid fluid flow of magnetized plasma, the energy and angular momentum flux per unit rest-mass flux

$$E = -T^{r}_{t}/(\rho_0 u^{r}) = -T^{\theta}_{t}/(\rho_0 u^{\theta}) \tag{B7}$$

and

$$L = T^{r}_{\phi}/(\rho_0 u^{r}) = T^{\theta}_{\phi}/(\rho_0 u^{\theta}), \tag{B8}$$

respectively, are conserved along each flow line. For unmagnetized flows E is conserved for any stationary flow, while L is conserved for any axisymmetric flow. If the ideal MHD approximation ($e^{\mu} = 0$) holds, then the magnetic flux per unit rest-mass flux

$$\Phi = \frac{B^{r}}{\rho_0 u^{r}} = \frac{B^{\theta}}{\rho_0 u^{\theta}} = \frac{B^{\phi}}{\rho_0(u^{\phi} - u^{t}\Omega_F)} \tag{B9}$$

is conserved along each flow line. This also implies that $(\Phi + b^{t})/\rho_0 = b^{r}/v^{r} = b^{\theta}/v^{\theta}$. Bekenstein & Oron (1978) also show that

$$\Psi = -E + \Omega_F L = h(u_t + \Omega_F u_{\phi}), \tag{B10}$$

is conserved along each flow line. One can reduce E and L to forms such as

$$E = -\zeta u_t - \Psi\Phi b_t/h = -hu_t + \Phi\Omega_F B_\phi \tag{B11}$$

$$L = \zeta u_\phi + \Psi\Phi b_\phi/h = hu_\phi + \Phi B_\phi \tag{B12}$$

where $h = (\rho_0 + u_g + p)/\rho_0$ is the gas specific enthalpy and $\zeta = h + b^2/\rho_0$ is the total specific enthalpy. Notice that for an isentropic flow that $d(\rho_0 + u)/d\rho_0 = h$ and so

$$dp/(h\rho_0) = dh/h. \tag{B13}$$

Clearly any ratio of these conserved flow quantities is also conserved along each flow line (e.g. the energy flux per unit magnetic flux (E/Φ)). Any axisymmetric, stationary flow solution can be written in terms of the 6 independent quantities A_ϕ, B^ϕ, Ω_F, Φ, E, and L, where the single function A_ϕ determines the dependent quantities B^r and B^θ. Entropy is a dependently conserved quantity when one writes the rest-mass density and enthalpy in terms of the entropy and another conserved quantity. In general, the solution is determined once the conserved flow quantities are set by the boundary conditions and the other quantities are set by the equations of motion, either directly or using the Grad-Shafranov approach (for a review see, e.g., Levinson 2005). The limitations of, and hence extensions to, the ideal MHD approximation are described in Meier (2004).

Note that for an axisymmetric stationary degenerate fluid the Boyer-Lindquist coordinate components are related to the Kerr-Schild coordinates by $B^r[\mathrm{BL}] = B^r[\mathrm{KS}]$, $B^\theta[\mathrm{BL}] = B^\theta[\mathrm{KS}]$,$B^\phi[\mathrm{BL}] = B^\phi[\mathrm{KS}] - B^r[\mathrm{KS}](a - 2r\Omega_F)/\Delta$, while for a general fluid $B_r[\mathrm{BL}] = B_r[\mathrm{KS}] + (aB_\phi)/\Delta$, $B_\theta[\mathrm{BL}] = B_\theta[\mathrm{KS}]$, and $B_\phi[\mathrm{BL}] = B_\phi[\mathrm{KS}]$.

C. IDEAL MHD FLUID FORCES

First, to investigate the spatial acceleration of the fluid along a flow line A_ϕ one requires a unit length space-like vector that satisfies $V^\mu A_{\phi,\mu} = 0$ since A_ϕ is conserved along a flow line. The unit-length magnetic field satisfies these properties since $B^\mu A_{\phi,\mu} = 0$. To study the poloidal acceleration along a field line, the toroidal magnetic field component it projected out to obtain the unit vector

$$B_p^{\hat{\mu}} = NB_p^\mu = N(B^\mu - \frac{(\omega^\phi_\nu B^\nu)\xi^\mu_\phi}{|\omega^\phi||\xi_\phi|}) = N(B^\mu - B^\phi\delta^\mu_\phi) \tag{C1}$$

where $N = 1/\sqrt{B_p^\mu B_p^\nu g_{\mu\nu}} = 1/\sqrt{B^i B^j g_{ij}}$ with $\{i,j\} = \{r,\theta\}$ only, and ω^ϕ is the ϕ basis one-form. Therefore the projection of an acceleration along a poloidal projection of each flow line is

$$a_{A_\phi} = a_\mu B_p^{\hat{\mu}} = a_r B^{\hat{r}} + a_\theta B^{\hat{\theta}} \tag{C2}$$

Second, to investigate the spatial collimation of the fluid, a unit length space-like vector that is perpendicular to the poloidal field line and perpendicular to the ϕ-direction (i.e. ξ_ϕ) is required. This vector is

$$C^{\hat{\mu}} = N_C C^\mu = N_C \epsilon^\mu_{\alpha\beta} B_p^{\hat{\alpha}} \xi^\beta_\phi, \tag{C3}$$

where $N_C = 1/\sqrt{C^\mu C^\nu g_{\mu\nu}}$ and $\epsilon^\mu{}_{\alpha\beta}$ is the spatial permutation tensor. Thus $C^{\hat{r}} = NN_C B^\theta$ and $C^{\hat{\theta}} = NN_C B^r$. Therefore the projection of an acceleration in the collimation direction is

$$a_{coll} = a_\mu C^{\hat{\mu}} = N_C(a_r B^{\hat{\theta}} - a_\theta B^{\hat{r}}). \tag{C4}$$

Notice that for $\theta < \pi/2$ if $a_{coll} < 0$, then the flow is collimating toward the polar axis. For $\theta > \pi/2$ if $a_{coll} > 0$, then the flow is collimating toward the polar axis.

Third, there are many interesting frames to measure the acceleration. The acceleration away from geodesics is obtained from the projection of $P^{\mu\nu} = g^{\mu\nu} + u^\mu u^\nu$ on $\nabla_\gamma T^\gamma_\mu = 0$, giving Euler's equations for the deviation from geodesic motion

$$\rho_0 h a^G_\mu = -P_\mu{}^\alpha p_{,\alpha} + J^\alpha F_{\alpha\mu} \tag{C5}$$

where $a^\mu_G = u^\mu_{;\nu}u^\nu = u^\alpha(u^\mu_{,\alpha} + \Gamma^\mu{}_{\beta\alpha}u^\beta)$ is the "geodesic acceleration" away from the geodesic motion ($a^\mu_G = 0$). Note that Γ here is the connection coefficient and not the Lorentz factor. This comoving geodesic acceleration "hides" the effect of gravity on the fluid. One could instead focus on the coordinate acceleration $a^\mu_C = u^\nu u^\mu_{,\nu}$, which represents the change in the 4-velocity in the momentarily comoving frame. From the geodesic equation of motion,

$$a^\mu_C = a^\mu_G - \Gamma^\mu{}_{\alpha\beta}u^\alpha u^\beta, \tag{C6}$$

and so the coordinate acceleration along a flow line is

$$a^C_{A_\phi} = a^C_\mu B_p^{\hat{\mu}} = a^G_{A_\phi} - B^{\hat{\mu}} u^\alpha u^\beta \Gamma_{\mu\alpha\beta}, \tag{C7}$$

so the geodesic deviation and gravitational acceleration along each flow line can be studied separately.

Notice that for a stationary flow $a^C_{A_\phi} = 0$ where the poloidal velocity $u^p = 0$. For a black hole with field lines that tie the black hole to large radii, there must exist a region where $u^p = 0$. For an outflow to reach large distances, the region where $u^p = 0$ separates those fluid elements that eventually fall into the black hole and those fluid elements that reach large distances. Levinson

(2005) refers to this as the “injection surface.” If particles were created only due to reaching the Goldreich-Julian charge density, then this must be the location where particles emerge. For an injection region with negligible angular velocity $u^{\phi} \approx 0$, then

$$a^G_{A_\phi} \approx B^{\hat{r}}\Gamma_{rtt} + B^{\hat{\theta}}\Gamma_{\theta tt} \tag{C8}$$

determines the location of the stagnation surface. In Boyer-Lindquist coordinates

$$\Gamma_{rtt} = \frac{r^2 - (a\cos\theta)^2}{\Sigma^2} \tag{C9}$$

and

$$\Gamma_{\theta tt} = -\frac{2ra^2\cos\theta\sin\theta}{\Sigma^2}. \tag{C10}$$

See section 3 for a discussion of injection physics.

C.1. *Forces in Lab Frame*

The forces as written in the lab frame, rather than comoving frame, allow for simple understanding of the force dynamics. Equations C5 and C2 imply that

$$a^G_{A_\phi} = NB^j(a^{G(MA)}_j + a^{G(EM)}_j), \tag{C11}$$

where for a stationary, axisymmetric flow

$$a^{G(MA)}_j = \frac{-u_j u^i p_{,i} + p_{,j}}{\rho_0 h} \tag{C12}$$

is the hydrodynamic acceleration. For an isentropic flow, equation B13 implies that

$$a^{G(MA)}_j = P_j{}^i(\log h)_{,i} = -u_j u^i(\log h)_{,i} + (\log h)_{,j}. \tag{C13}$$

For an axisymmetric, stationary, ideal MHD fluid the electromagnetic acceleration $a^{G(EM)}_j = J^{\alpha}F_{\alpha j}/(\rho_0 h)$ reduces to simply

$$a^{G(EM)}_j = \frac{-B^{\phi}B_{\phi,j}}{\rho_0 h}. \tag{C14}$$

Thus the magnetic acceleration is due to the gradient of the toroidal magnetic field along a field line. Notice that from equation B11 or B12 that in the limit $\rho_0 h \rightarrow 0$ that $B_\phi \rightarrow E/(\Phi\Omega_F) = L/\Phi$, a conserved flow quantity, thus $B^j B_{\phi,j} = 0$ implying the electromagnetic field is force-free. However, notice that the acceleration $a^{G(EM)}_j$ then becomes undefined.

Equations C5 and C4 imply that

$$a^G_{coll} = NN_C B^j(a^{G(MA)}_k + a^{G(EM)}_k)\epsilon^k{}_j, \tag{C15}$$

where $\epsilon^k{}_j$ is the poloidal permutation tensor and $a^{G(MA)}_k$ is given in equations C12 or C13. This hydrodynamic collimation is due to the pressure acceleration in the comoving frame along a field line but directed to collimate the flow. For an axisymmetric, stationary, ideal MHD fluid the electromagnetic collimation acceleration ($C^{\hat{j}}J^{\alpha}F_{\alpha j}/(\rho_0 h) = C^{\hat{j}}a^{G(EM)}_j$) reduces to

$$a^G_{coll}{}^{(EM)} = \frac{NN_C}{\rho_0 h}\left(\epsilon^{ab}(B^p)^2 f[B_a] + \epsilon_a{}^b B^a B^{\phi} B_{\phi,b}\right), \tag{C16}$$

where $f[B_a] \equiv \left(B_{a,b} - \Omega_F(\tau_a B_a)_{,b}\right)$ and $(B^p)^2 \equiv (B^r)^2 + (B^\theta)^2$ and $\epsilon_a{}^b$ is the poloidal permutation tensor. The last term on the right hand side of equation C16 represents the “hoop-stress” that leads to collimation for nonrelativistic winds. The first two terms on the right hand side correspond, respectively, to the forces due to poloidal magnetic stresses and the electric field (E^i) gradients. The latter can collimate relativistic outflows.

D. COMPTON SCATTERING

In the lab frame, seed photons are Compton upscattered if the energy of the photon $E_{seed} \ll \Gamma_e m_e c^2$ for an electron Lorentz Γ_e. The upscattering continues until the lab frame photon energy exceeds electron energy. In the lab frame, each scatter gives the photon a new energy $E_{scat} \approx 4\Gamma_e^2 E_{seed}$ if $E_{seed} < m_e c^2/\Gamma_e$ and $E_{scat} \approx \Gamma_e m_e c^2$ otherwise. Two limiting scenarios are if the photon crosses the jet or if the photon travels parallel and within the jet.

The optical depth to Compton scattering for a photon in the rest frame of the jet electrons is

$$\tau = \int_{l'} \left(\frac{\rho_{0,e^-e^+}}{m_e}\right)\sigma_T dl', \tag{D1}$$

which in the lab frame gives

$$\tau = \int_{l} \left(\frac{\rho_{0,e^-e^+}}{m_e}\right)\sigma_T \Gamma_e(1-\beta\cos\theta)dl, \tag{D2}$$

where $\beta = v/c$, $\Gamma_e = (1-\beta^2)^{-1/2}$, and $\theta = \pi/2$ corresponds to perpendicular interactions and $\theta = 0$ to parallel. Across the jet

$$\tau_\perp = \int_{-\theta_j}^{\theta_j} \left(\frac{\rho_{0,e^+e^-}}{m_e}\right) \sigma_T \Gamma_e r d\theta, \tag{D3}$$

while for along the jet

$$\tau_\parallel = \int_{r_0}^{\infty} \left(\frac{\rho_{0,e^-e^+}}{m_e}\right) \sigma_T \Gamma_e (1-\beta) dr, \tag{D4}$$

where $\beta = \left(\frac{\Gamma_e^2-1}{\Gamma_e^2}\right)^{1/2}$. For $\Gamma_e \gg 1$, $\Gamma_e(1-\beta) \approx (2\Gamma_e)^{-1}$, so

$$\tau_\parallel \approx \int_{r_0}^{\infty} \left(\frac{\rho_{0,e^+e^-}}{m_e}\right) \left(\frac{\sigma_T}{2\Gamma_e}\right) dr, \tag{D5}$$

where σ_T is the Thomson scattering cross-section and r_0 is some fiducial starting radius in the jet (see Rybicki & Lightman 1979; Longair 1992).

Similar calculations can be used to estimate the forward or backwards pair-production or pair-annihilation optical depths. In the lab frame, for a photon gas moving with Γ with one photon energy $E = \Gamma E'$ and another $> (\Gamma m_e c^2)^2/E$, then the photons annihilate with a cross section at $E \lesssim 0.5$MeV of $\sigma \approx \sigma_T$ and the Klein-Nishina corrections for photons with $E \gtrsim 0.5$MeV modify the cross section such that $\sigma \propto E^{-1}$. For a spectrum (number per unit time per unit area per unit energy) $fE^{-\alpha}$, then for $\alpha = 2$, the average cross section is $\sigma \approx 0.06\sigma_T$. In this case the relevant proper density is n_γ when for a photon beam, where n_γ is the number density of (typically fewer) high energy photons. See also Lithwick & Sari (2001).

For a beam of electrons with velocity β, $\sigma \approx \sigma_T/\beta$ for nonrelativistic electrons and for $\Gamma \gg 1$

$$\sigma \approx \frac{3\sigma_T}{8\Gamma}(\log 2\Gamma - 1). \tag{D6}$$

The pair annihilation rate is

$$t_{pa}^{-1} \approx \langle \sigma v \rangle \left(\frac{\rho_{0,e^-e^+}}{m_e}\right), \tag{D7}$$

which can be compared to some dynamical time to determine if pair annihilation is important.

REFERENCES

Abramowicz, M., Jaroszinski, M., & Sikora, M. 1978, A&A, 63, 221
Achterberg, A., Gallant, Y. A., Kirk, J. G., & Guthmann, A. W. 2001, MNRAS, 328, 393
Akiyama, S., Wheeler, J. C., Meier, D. L., & Lichtenstadt, I. 2003, ApJ, 584, 954
Bardeen, J. M. 1970, ApJ, 161, 103
Begelman, M. C., Blandford, R. D., & Rees, M. J. 1984, Rev. Mod. Phys., 56, 255
Begelman, M. C., & Sikora, M. 1987, ApJ, 322, 650
Begelman, M. C., Rees, M. J., & Sikora, M. 1994, ApJ, 429, L57
Begelman, M. C. 1998, ApJ, 493, 291
Begelman, M. C., Ergun, R. E., & Rees, M. J. 2005, ApJ, 625, 51
Bekenstein, J. D., & Oron, E. 1978, Phys. Rev. D, 18, 1809
Biretta, J. A., Sparks, W. B., & Macchetto, F. 1999, ApJ, 520, 621
Biretta, J. A., Junor, W., & Livio, M. 2002, New Astronomy Review, 46, 239
Bisnovatyi-Kogan, G. S., & Ruzmaikin, A. A. 1976, Ap&SS, 42, 401
Blandford, R. D. 1976, MNRAS, 176, 465
Blandford, R., & Eichler, D. 1987, Phys. Rep., 154, 1
Blandford, R. D. & Znajek, R. L. 1977, MNRAS, 179, 433
Broderick, A. E. 2004, astro-ph/0411778
Celotti, A., & Fabian, A. C. 1993, MNRAS, 264, 228
Chaty, S., Charles, P. A., Martí, J., Mirabel, I. F., Rodríguez, L. F., & Shahbaz, T. 2003, MNRAS, 343, 169
Coburn, W. & Boggs, S. E. 2003, Nature, 423, 415
De Villiers, J., Hawley, J. F., Krolik, J. H., & Hirose, S. 2005, ApJ, 620, 878
Di Matteo, T., Perna, R., & Narayan, R. 2002, ApJ, 579, 706
Di Matteo, T., Springel, V., & Hernquist, L. 2005, Nature, 433, 604
Duncan, R. C. & Thompson, C. 1992, ApJ, 392, L9
Eichler, D. 1993, ApJ, 419, 111
Elvis, M. 2000, ApJ, 545, 63
Elvis, M., Risaliti, G., & Zamorani, G. 2002, ApJ, 565, L75
Elvis, M., Risaliti, G., Nicastro, F., Miller, J. M., Fiore, F., & Puccetti, S. 2004, ApJ, 615, L25
Fabian, A. C., et al. 2002, MNRAS, 335, L1
Feldman, W. C., & Marsch, E.: 1997, in J. R. Jokipii, C. P. Sonett, and M. S. Giampapa (eds.), Cosmic Winds and the Heliosphere, Univ. of Arizona Press, Tucson, 617.
Fender, R. 2003, astro-ph/0303339
Fender, R., & Maccarone, T. 2003, astro-ph/0310538
Fender, R., Maccarone, T., & van Kesteren, Z. 2005, astro-ph/0504205
Fender, R., & Belloni, T. 2004, ARA&A, 42, 317
Fender, R. P., Belloni, T. M., & Gallo, E. 2004, MNRAS, 355, 1105
Foster, R. S., Waltman, E. B., Tavani, M., Harmon, B. A., Zhang, S. N., Paciesas, W. S., & Ghigo, F. D. 1996, ApJ, 467, L81
Frank, J., King, A., & Raine, D. 2002, (New York: Cambridge) §9.7.
Gaidos, J. A., et al. 1996, Nature, 383, 319
Gammie, C. F., McKinney, J. C., & Gábor Tóth 2003, ApJ, 589, 444
Gammie, C. F., Shapiro, S. L., & McKinney, J. C. 2004, ApJ, 602, 312
Gierliński, M., & Done, C. 2004, MNRAS, 347, 885
Ghirlanda, G., Celotti, A., & Ghisellini, G. 2003, A&A, 406, 879
Ghirlanda, G., Ghisellini, G., & Lazzati, D. 2004, ApJ, 616, 331
Ghirlanda, G., Ghisellini, G., Firmani, C., Celotti, A., & Bosnjak, Z. 2005, MNRAS, L31
Ghisellini, G., Celotti, A., George, I. M., & Fabian, A. C. 1992, MNRAS, 258, 776
Ghisellini, G., Padovani, P., Celotti, A., & Maraschi, L. 1993, ApJ, 407, 65
Ghisellini, G., & Madau, P. 1996, MNRAS, 280, 67
Ghisellini, G., Lazzati, D., Celotti, A., & Rees, M. J. 2000, MNRAS, 316, L45
Ghisellini, G., & Celotti, A. 2001, MNRAS, 327, 739
Ghisellini, G., & Celotti, A. 2002, Blazar Astr. w/BeppoSAX, 257
Ghisellini, G. 2003, astro-ph/0310168
Ghisellini, G., Haardt, F., & Matt, G. 2004, A&A, 413, 535
Ghisellini, G., Tavecchio, F., & Chiaberge, M. 2005, A&A, 432, 401
Ghosh, P. & Abramowicz, M. A. 1997, MNRAS, 292, 887
Goldreich, P., & Julian, W. H. 1969, ApJ, 157, 869
Goodman, J. 1997, New Astronomy, 2, 449
Granot, J. & Königl, A. 2003, ApJ, 594, L83
Greiner, J., Cuby, J. G., & McCaughrean, M. J. 2001, Nature, 414, 522
Guilbert, P. W., Fabian, A. C., & Rees, M. J. 1983, MNRAS, 205, 593
Hardcastle, M. J. 2005, X-Ray and Radio Connections (eds. L.O. Sjouwerman and K.K Dyer) Published electronically by NRAO, http://www.aoc.nrao.edu/events/xraydio Held 3-6 February 2004 in Santa Fe, New Mexico, USA, (E7.03) 8 pages,

Hirose, S., Krolik, J. H., De Villiers, J., & Hawley, J. F. 2004, ApJ, 606, 1083
Hjorth, J., et al. 2003, Nature, 423, 847
Ho, L. C. 1999, ApJ, 516, 672
Igumenshchev, I. V., & Abram owicz, M. A. 1999, MNRAS, 303, 309.
Igumenshchev, I. V., & Abram owicz, M. A. 2000, ApJS, 130, 463.
Igumenshchev, I. V., Narayan, R., & Abramowicz, M. A. 2003, ApJ, 592, 1042
Jorstad, S. G., Marscher, A. P., Mattox, J. R., Wehrle, A. E., Bloom, S. D., & Yurchenko, A. V. 2001, ApJS, 134, 181
Junor, W., Biretta, J. A., & Livio, M. 1999, Nature, 401, 891
Kaiser, C. R., Gunn, K. F., Brocksopp, C., & Sokoloski, J. L. 2004, ApJ, 612, 332
Kawabata, K. S., et al. 2003, ApJ, 593, L19
Keshet, U., & Waxman, E. 2005, Physical Review Letters, 94, 111102
Kino, M., & Takahara, F. 2004, MNRAS, 349, 336
Khokhlov, A. M., Höflich, P. A., Oran, E. S., Wheeler, J. C., Wang, L., & Chtchelkanova, A. Y. 1999, ApJ, 524, L107
Kohri, K., & Mineshige, S. 2002, ApJ, 577, 311
Kohri, K., Narayan, R., & Piran, T. 2005, astro-ph/0502470
Koide, S., Shibata, K., Kudoh, T., & Meier, D. L. 2002, Science, 295, 1688
Komissarov, S. S. 2005, MNRAS, 359, 801
Konopelko, A., Mastichiadis, A., Kirk, J., de Jager, O. C., & Stecker, F. W. 2003, ApJ, 597, 851
Kouveliotou, C., et al. 1999, ApJ, 510, L115
Krasnopolsky, R. et al., 2005, in prep.
Krawczynski, H., Coppi, P. S., & Aharonian, F. 2002, MNRAS, 336, 721
Krichbaum, T. P., et al. 2004, European VLBI Network on New Developments in VLBI Science and Technology, 15
Lazzati, D., Rossi, E., Ghisellini, G., & Rees, M. J. 2004, MNRAS, 347, L1
Leblanc, J. M. & Wilson, J. R. 1970, ApJ, 161, 541
Levinson, A., & Blandford, R. 1996, ApJ, 456, L29
Levinson, A., & Eichler, D. 1993, ApJ, 418, 386
Levinson, A., & Eichler, D. 2003, ApJ, 594, L19
Levinson, A. 2005, astro-ph/0502346
Lewin, W. H. G., van Paradijs, J., & van den Heuvel, E. P. J. 1995, Cambridge Astrophysics Series, Cambridge, MA: Cambridge University Press, |c1995, edited by Lewin, Walter H.G.; Van Paradijs, Jan; Van den Heuvel, Edward P.J.,
Ling, J. C., & Wheaton, W. A. 2005, ApJ, 622, 492
Lithwick, Y., & Sari, R. 2001, ApJ, 555, 540
Livio, M., Ogilvie, G. I., & Pringle, J. E. 1999, ApJ, 512, 100
Longair, M. S. 1992, Cambridge: Cambridge University Press, 1992, 2nd ed.,
Lopez, L. A., Marshall, H. L., Kane, J. F., Schulz, N. S., & Canizares, C. R. 2003, American Astronomical Society Meeting Abstracts, 203,
Lorimer, D. R. 2001, astro-ph/0104388
Lovelace, R. V. E. 1976, Nature, 262, 649
Lyutikov, M., Pariev, V. I., & Blandford, R. D. 2003, ApJ, 597, 998
MacDonald, D. & Thorne, K. S. 1982, MNRAS, 198, 345
MacFadyen, A. I. & Woosley, S. E. 1999, ApJ, 524, 262
MacFadyen, A. I., Woosley, S. E. & Heger, A. 2001, ApJ, 550, 410
Martocchia, A., Matt, G., Karas, V., Belloni, T., & Feroci, M. 2002, A&A, 387, 215
McClintock, J. E., & Remillard, R. A. 2003, astro-ph/0306213
McKinney, J. C., & Gammie, C. F. 2002, ApJ, 573, 728
McKinney, J.C. 2004, unpublished Ph.D. thesis, University of Illinois at Urbana-Champaign, http://rainman.astro.uiuc.edu/˜jon/research/thesis.pdf
McKinney, J. C., & Gammie, C. F. 2004, ApJ, 611, 977
McKinney, J. C. 2005a, astro-ph/0506367
McKinney, J. C. 2005b, astro-ph/0506369
Meier, D. L. 2001, ApJ, 548, L9
Meier, D. L. 2003, New Astronomy Review, 47, 667
Meier, D. L. 2004, ApJ, 605, 340
Merloni, A., Heinz, S., & di Matteo, T. 2003, MNRAS, 345, 1057
O. E. B. Messer, A. Mezzacappa, S. W. Bruenn, and M. W. Guidry, Astrophys. J. **507**, 353 (1998); S. Yamada, H-Th Janka, H. Suzuki, Astron. Astrophys. **344**, 533 (1999); A. Burrows, T. Young, P. Pinto, R. Eastman, T. A. Thompson, Astrophys. J. **539**, 865 (2000); M. Rampp, H-Th Janka, Astrophys. J. **539**, L33 (2000); M. Liebendoerfer, *et al.* Phys. Rev. D **63**, 104003-1 (2001).
Mészáros, P. 2002, ARA&A, 40, 137
Mészáros, P. & Rees,M. J. 1997, ApJ, 482, L29
Mirabel, I. F., Rodriguez, L. F., Cordier, B., Paul, J., & Lebrun, F. 1992, Nature, 358, 215
Mirabel, I. F., & Rodriguez, L. F. 1994, Nature, 371, 46
Mirabel, I. F., & Rodríguez, L. F. 1999, ARA&A, 37, 409
Mizuno, Y., Yamada, S., Koide, S., & Shibata, K. 2004, ApJ, 615, 389
Narayan, R., Paczynski, B., & Piran, T. 1992, ApJ, 395, L83
Narayan, R. & Yi, I. 1995, ApJ, 452, 710
Narayan, R., Piran, T., & Kumar, P. 2001, ApJ, 557, 949
Narayan, R., Igumenshchev, I. V., & Abramowicz, M. A. 2003, PASJ, 55, L69
Nishikawa, K.-I., Hardee, P., Richardson, G., Preece, R., Sol, H., & Fishman, G. J. 2003, ApJ, 595, 555
Noble, S.C. , Gammie, C.F., McKinney, J.C., Del Zanna, L.D., 2005, submitted.
Okamoto, I. 1999, MNRAS, 307, 253
Okamoto, I. 2000, MNRAS, 318, 250
Shu, C.W., 1997, NASA/CR-97-206253, No.97-65
Paczynski, B. 1998, ApJ, 494, L45
Phinney, E.S. 1983, unpublished Ph.D. thesis, Cambridge University
Piran, T. 2005, Reviews of Modern Physics, 76, 1143
Popham, R., Woosley, S. E., & Fryer, C. 1999, ApJ, 518, 356
Punch, M., et al. 1992, Nature, 358, 477
Punsly, B., & Coroniti, F. V. 1990, ApJ, 354, 583
Punsly, B., & Coroniti, F. V. 1990, ApJ, 350, 518
Punsly, B. 1991, ApJ, 372, 424
Punsly, B. 2001, Black hole gravitohydromagnetics, Berlin: Springer, 2001, xii, 400 p., Astronomy and astrophysics library, ISBN 3540414665,
Ramirez-Ruiz, E., & Socrates, A. 2005, astro-ph/0504257
Rees, M. J., Phinney, E. S., Begelman, M. C., & Blandford, R. D. 1982, Nature, 295, 17
Reynolds, C. S., di Matteo, T., Fabian, A. C., Hwang, U., & Canizares, C. R. 1996, MNRAS, 283, L111
Ruderman, M. A., & Sutherland, P. G. 1975, ApJ, 196, 51
Ruffini, R., & Wilson, J. R. 1975, Phys. Rev. D, 12, 2959
Rybicki, G. B., & Lightman, A. P. 1979, New York, Wiley-Interscience, 1979. 393 p.,
Salpeter, E. E. 1964, ApJ, 140, 796
Shakura, N. I., & Sunyaev, R. A. 1973, A&A, 24, 337
Shapiro, S. L. & Shibata, M. 2002, ApJ, 577, 904
Shibata, M. & Shapiro, S. L. 2002, ApJ, 572, L39
Shapiro, S. L. 2005, ApJ, 620, 59
Shu, F. H. 1992, Physics of Astrophysics, Vol. II, by Frank H. Shu. Published by University Science Books, ISBN 0-935702-65-2, 476pp, 1992.,
Sikora, M., Begelman, M. C., Madejski, G. M., & Lasota, J. 2005, ApJ, 625, 72
Sikora, M., & Madejski, G. 2000, ApJ, 534, 109
Soderberg, A. M. & Ramirez-Ruiz, E. 2003, AIP Conf. Proc. 662: Gamma-Ray Burst and Afterglow Astronomy 2001: A Workshop Celebrating the First Year of the HETE Mission, 662, 172
Sol, H., Pelletier, G., & Asseo, E. 1989, MNRAS, 237, 411
Springel, V., Di Matteo, T., & Hernquist, L. 2004, astro-ph/0411108
Stone, J. M., Pringle, J. E., & Begelman, M. C. 1999, MNRAS, 310, 1002.
Stone, J. M. & Pringle, J. E. 2001, MNRAS, 322, 461
Symbalisty, E. M. D. 1984, ApJ, 285, 729
Stanek, K. Z., et al. 2003, ApJ, 591, L17
Taylor, G. B., Frail, D. A., Berger, E., & Kulkarni, S. R. 2004, ApJ, 609, L1
Taylor, G. B., Momjian, E., Pihlstrom, Y., Ghosh, T., & Salter, C. 2004, astro-ph/0412483
Tanaka, Y., et al. 1995, Nature, 375, 659
Thompson, C., & Duncan, R. C. 1995, MNRAS, 275, 255
Thompson, C., & Duncan, R. C. 1996, ApJ, 473, 322
Thorne, K. S. 1974, ApJ, 191, 507
Thorne, K. S., & MacDonald, D. 1982, MNRAS, 198, 339
Thorne, K. S., Price, R. H., & MacDonald, D. A. 1986, Black Holes: The Membrane Paradigm
Thorsett, S. E., & Chakrabarty, D. 1999, ApJ, 512, 288
Tsinganos, K., & Bogovalov, S. 2005, AIP Conf. Proc. 745: High Energy Gamma-Ray Astronomy, 745, 148
Uemura, M., et al. 2003, Nature, 423, 843
Urry, C. M., & Padovani, P. 1995, PASP, 107, 803
Usmanov, A. V., Goldstein, M. L., Besser, B. P., & Fritzer, J. M. 2000, J. Geophys. Res., 105, 12675
Uzdensky, D. A., & Spruit, H. C. 2005, astro-ph/0504429
Wald, R. M. 1974, ApJ, 191, 231
Wang, L. & Wheeler, J. C. 1996, ApJ, 462, L27
Wang, L., Howell, D. A., Höflich, P., & Wheeler, J. C. 2001, ApJ, 550, 1030
Wang, L., et al. 2002, ApJ, 579, 671
Wang, L., Baade, D., Höflich, P., & Wheeler, J. C. 2003, ApJ, 592, 457
Wheeler, J. C., Yi, I., Höflich, P., & Wang, L. 2000, ApJ, 537, 810
Woosley, S. E. 1993, ApJ, 405, 273
Woosley, S. E. & Weaver, T. A. 1986, ARA&A, 24, 205
Zel'dovich Y. B. 1964, Sov. Phys.-Dokl., 9, 195
Zhang, W., & MacFadyen, A. I. 2005, astro-ph/0505481